The Design of a Flexible Friction-Based Tissue Transporting Device for Minimally Invasive Surgery

by

Mike van Zelm

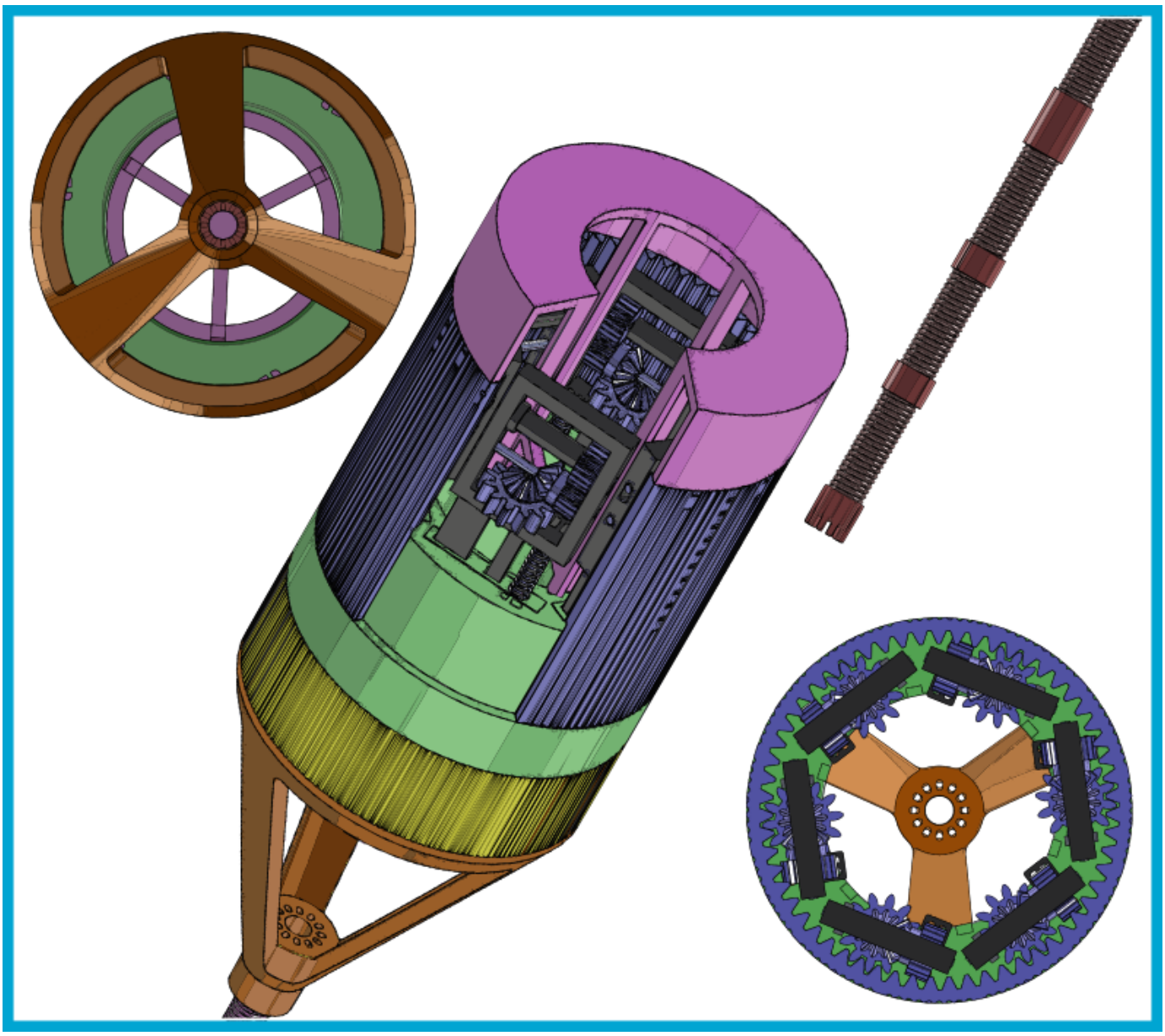

TU Delft

The Design of a Flexible Friction-Based Tissue Transporting Device for Minimally Invasive Surgery

by

Mike S.R. van Zelm

25 November 2024

to obtain the degree of
MSc Mechanical Engineering
at the Delft University of Technology

to be defended on
the 6th of December 2024 at 09:00

Student number:	4725387
Project duration:	September 2023 - November 2024
Thesis supervisors:	Dr. A. Sakes
	Ir. V. Kortman
Thesis committee:	Dr. A. Sakes (chair)
	Dr.Ir. R.M. Oosting
	Ir. V.G. Kortman

TU Delft

Acknowledgments

Writing this thesis was no easy task, especially as it was mostly on my own. Luckily, I had people surrounding me to motivate and support me. I would like to dedicate this chapter to thank everyone who helped me during this project.

First of all, I would like to thank my supervisors for their guidance during my project: Dr. Aimée Sakes and Ir. Vera Kortman. I always enjoyed our productive meetings; from our first online meeting when I was in Barcelona, to the meetings in the office, the online meetings when both of you were in Tokyo, and the final meetings we had in the office again. The meetings gave me insightful feedback to improve my work, while also having room for little side talks and fun stories. We could always discuss any matter and express our opinions clearly, tackling the challenges ahead with optimism and enthusiasm. We were easily able to make agreements on design choices or work to be done. An unusual agreement we made was all of us taking a three month break to go to Asia, the two of you for a project in Tokyo and me going on the adventure of a lifetime. I am grateful that I have had you as supervisors.

Secondly, I would like to thank my family. They have always supported me and motivated me to achieve my full potential, giving me whatever I needed to succeed. They have been there from the very start, and remain to stay a strong motivation for me to make them proud. Thirdly, I would like to thank my girlfriend, Sujata, who would always listen to my doubts, complaints, and whatever I had to share about my thesis. You would give me useful feedback, be there to listen, or be just as enthusiastic as me about my newly 3D-printed parts. Besides, I want to thank my friends for the encouragement, support, and standing by my side through the highs and lows. My friends have been an unchangeable part of this journey. Whether I met these friends during my masters, my exchanges, my bachelors or during high school, you made this journey not only achievable but also enjoyable and memorable. Finally, I would like to thank me for believing in me, for doing all the hard work, and for never quitting.

As my student time is now over, I will have to leap into adult life, and look for a job. During my student time, I accumulated incredibly valuable experiences and lessons. All these moments are what makes me who I am today, and I will carry all of this with me to the future. To you, reading this thesis now, I wish you lots of joy reading about the topic that I have worked on for over a year.

CONTENTS

***Abstract*—The removal of tissues from the human body is a fundamental aspect of surgical interventions, especially in Minimally Invasive Surgery (MIS). In MIS, one or multiple small incisions (approximately 3 to 10 mm) are made, and the body is accessed by long slender devices. MIS offers benefits such as less postoperative pain, and shorter hospital stays, driving a trend toward miniaturisation: smaller medical instruments. Current suction-based instruments are limited in performance by clogging, shaft miniaturisation challenges, and dependency on tissue composition. To address these limitations, alternative mechanisms for transportation have arisen such as friction-based transportation. This study presents the design and experimental validation of a flexible friction-based tissue transporting device for MIS. The device is designed to achieve transportation efficiency independent of tissue elasticity within a Young's modulus range of 1-110 kPa, utilising a cylindrical conveyor mechanism with wires to transport tissue. Experimental validation demonstrated consistent transportation efficiency (75%) across various tissue types, shapes, and orientations, though shaft curvature significantly affected performance and total reliability (81%). The device addresses some of the limitations of suction-based instruments, including reduced clogging, enhanced potential for miniaturisation, and transportation efficiency independent of tissue elasticity. While further improvements to the device design are necessary, it has the potential to improve MIS tissue removal procedures and patient outcomes.**

***Index Terms*—Minimally Invasive Surgery (MIS), tissue transportation, friction-based transport, medical device design**

I. Introduction

A. Tissue Removal

The removal of tissues from the human body is a fundamental aspect of surgical interventions. This integral component of surgical practice plays a pivotal role in diagnostic and therapeutic procedures, spanning a large variety of medical specialities. Whether it is the precise extraction of abnormal tissue for pathological analysis or the controlled excision of diseased structures to restore health, the process of tissue removal has witnessed a constant evolution in techniques and technologies. Even so, the removal process remains a challenging task, as any nearby healthy tissue should not be damaged. Treatment often involves the transportation of the disturbance, such as infectious or cancerous tissue, from inside the body to the outside environment [1] [2].

Traditionally, tissue was removed during open surgery. With this method, a relatively large incision is made, making tissue removal a straightforward procedure. However, over the past two decades open surgery has slowly been replaced by MIS. In MIS, one or multiple small incisions (approximately 3 to 10 mm) are made, and the body is accessed by slender devices with a diameter between 2 to 5 mm. Using small incisions results in positive primary and secondary outcomes compared to traditional open surgery as it leads to reduced surgery duration, less pain after the operation, shorter hospital stays, and improved cosmetic outcome [3] [4]. The downside to MIS is, however, that the small incisions result in a longer path from the surgical incision to the operation site, and limited diameter for tissue removal. Therefore, the biggest challenge for MIS is the removal and especially the transportation of the tissue, from inside to outside the body. Furthermore, due to the positive primary and secondary effects of using small incisions, miniaturisation of medical instruments is the ongoing trend in surgery today.

B. Present-day equipment

Currently, tissue extraction in MIS is performed with flexible graspers and suction-based instruments. Suction-based instruments such as aspiration catheters and morcellators are the most commonly used devices for facilitating tissue transportation and they are therefore referred to as the golden standard [5]. Aspiration catheters consist of a flexible tubular shaft with diameters ranging from a few millimetres to a maximum of ten millimetres, containing a suction lumen. Figure 1 shows a section view of an aspiration catheter shaft. Transportation is achieved by applying a pressure gradient over the shaft. By applying a negative pressure at the proximal end of the catheter shaft, tissue in front of the distal end is pulled into the shaft, and transported to the proximal end. Tissue is pulled into the shaft only if the suction force exceeds the friction force between the tissue and the shaft, as well as the force at which the tissue is attached to its surroundings. By exerting a force on the catheter shaft at the proximal end, the tip of the catheter can be positioned at the target location for tissue extraction.

Although suction-based instruments are effective for the removal of liquids and incoherent tissues, they are less effective for solid or coherent tissues due to possible clogging of the instrument. A visual representation of clogging can be seen on the right of Figure 1. Clogging occurs when the friction forces between the tissue and the instrument walls exceed the suction force [7]. Stiffer clots are less likely to deform

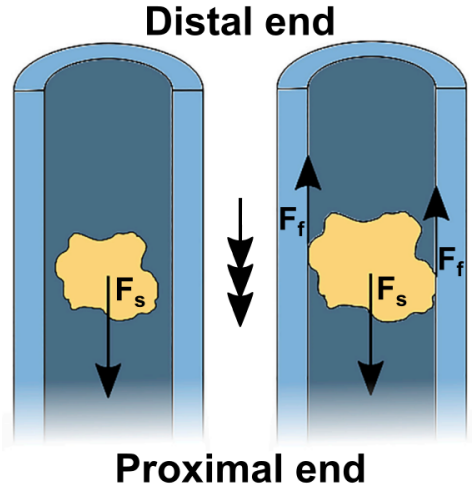

Fig. 1: Section view of suction-based transportation [6]. A suction force F_s acts on the tissue in the transport direction denoted by the triple arrow, clogging occurs if the resultant of friction forces F_f is larger than F_s. Clogging prevents further transportation of tissue.

and adjust their shape to the shaft, resulting in high forces with the shaft walls. Therefore, stiff tissue poses a higher risk of getting stuck within the shaft compared to softer tissue [8]. Clogging requires removal of the blockage, as further transportation of tissue is impossible and thus procedure time increases while reliability decreases. This is disadvantageous, as a shorter surgery duration is beneficial to reduce both time under anaesthesia and operational costs [5].

The ongoing trend nowadays in MIS is miniaturisation: instruments are reducing in size. For aspiration-based instruments, this is difficult as these instruments are dependent on the shaft cross sectional area to generate force. The suction force is dependent on the shaft cross sectional area and pressure gradient, force decreases drastically with smaller diameter. For the same suction force with a two times smaller shaft diameter, a four times larger pressure gradient is needed. Besides conventional suction-based instruments, new paradigms for tissue transport have arisen. The use of friction might be an interesting avenue, as friction with the walls of the device will cause transportation instead of resulting in clogging. Transportation using friction requires the friction force in the transport direction to be larger than the friction in the opposite direction. Friction-based transportation is viable but has mostly been used in rigid form and research settings. A rigid device is less desired, as a flexible device will be able to reach a greater target area in the human body, and can be interesting for the removal of tissue in a variety of surgeries including Ear Nose and Throat (ENT) or endonasal skull base surgery [6].

C. Goal

The goal of this study is to design a flexible friction-based continuous tissue transporting device compatible with MIS in which the transportation efficiency is independent of tissue elasticity within the Young's modulus range of 1-110 kPa. This tissue elasticity range represents a large span of different tissue that can be encountered during MIS. The scope of this study does not include the procedure of tissue collection, insertion, and extraction from the device. The emphasis of this research is the principle of tissue transportation, assuming that tissue is present in the tubular body.

II. State of the Art

A. Suction-based Transportation

Commercially available suction-based catheters use a pressure gradient over a tubular structure to exert a force on tissue, transportation occurs when the friction force on the tissue in the shaft is lower than the applied suction force. Figure 2 shows a schematic overview of an aspiration catheter shaft and the involved forces. The suction force can be calculated with Equation 1. Here, F (N) represents the suction force in Newton, P (N/M^2) the pressure, and A (m^2) the surface area of the aspiration port.

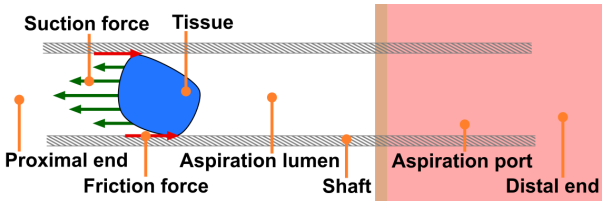

Fig. 2: Schematic overview of an aspiration catheter (the figure is not to scale). The part in light red will enter the human body.

$$F(N) = P(N/m^2) \cdot A(m^2) \tag{1}$$

The suction force depends on the product of the pressure gradient and shaft diameter, a larger diameter yields a higher suction force. As ongoing miniaturisation is desired, a dependence on diameter for force generation is disadvantageous. For the same suction force with a smaller diameter, a higher pressure gradient is needed. However, it is difficult to keep sufficient pressure gradient over the shaft while decreasing the diameter and increasing working length [9]. This is due to higher energy losses associated with the use of a smaller diameter shaft [10].

Suction-based instruments are effective for the removal of liquids and soft tissue but have difficulties removing and transporting rigid tissues. Rigid tissue has little deformation inside the tubular body which can lead to high friction and thus clogging, posing risks for operation of the device. Therefore, reliability of suction-catheters is dependent on tissue composition.

Aspiration-based instruments function generally well, but still pose multiple operational challenges which make it unsuitable for the removal of coherent tissues over long distances. For the future, a reliable and miniaturisable tissue transport mechanism is necessary which offers transportation independent of tissue composition or shaft diameter. Therefore, the implementation of new paradigms for tissue transportation seem interesting, this study will focus on friction-based transportation.

B. Friction-based Segmented Transportation

In a study by Sakes et al. [5], a wasp-inspired friction transportation device was developed with the goal to achieve a transportation rate and reliability independent of tissue composition. The transportation mechanism can be seen in Figure 3. The device is inspired by parasitic wasps, which lay eggs into their hosts by the insertion of a sting. Egg transportation inside the sting occurs by friction-based transport. Three segments can move independently with respect to each other, it is assumed that the total friction is divided equally over all three segments. When two segments move downward, the net friction in that direction is greater than the resistance of the single segment, and thus the egg is transported in the downward direction. The exact motion sequence is unknown,

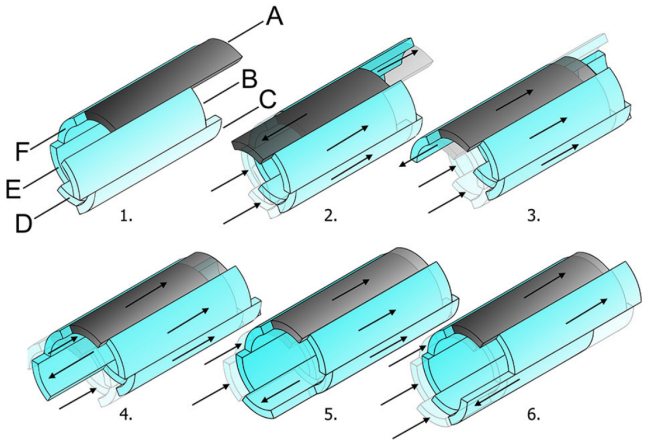

Fig. 3: Motion sequence of the device developed by Sakes et al. [5]. One blade is advanced, while the remaining blades are gradually retreated in a consecutive manner (1-6). The advancing blade moves one blade anticlockwise per actuation cycle (1-6).

but by varying which segments move up and down, a net direction of transport can be achieved.

The device contains six semi-cylindrical blades, which each can slide forwards and backwards. For this system to work, the majority of the blades should move in the transport direction at any one point in time. Depending on the amount of blades that slide in the transport direction, a resultant transportation force is generated on the tissue. By sequentially changing the blades that slide forward, continuous tissue transportation can be achieved.

In a follow-up study by De Kater et al. [6], a flexible version of the device from Sakes et al. [5] was developed. This device contains a ring of round cables that represent the blades, it can be seen in Figure 4. The eighteen flexible blades are segmented into six groups of three blades. The blades have a round shape such that the bending stiffness in any direction is equal. The device is flexible due to the use of blades and magnetic rings instead of a rigid shaft. The blades are surrounded by ring magnets, these attract the blades and make sure they stay in place, but still allow for movement. A thin plastic tube is wrapped around the outside to prevent tissue from escaping in between the blades. The blades can translate continuously in length direction, the motion sequence is that five groups move forward, while the sixth group moves backward. A disadvantage of the motion sequence of the device is that one group of blades is always moving against the direction of transportation, providing resistance to motion.

C. Friction-based Conveyor Transportation

Verberne et al. [11] developed a continuous friction-based tissue transporting device able to transport tissue through the tubular body by movement of multiple small wires. Figure 5 shows a schematic view of the device, mimicking the motion of a conveyor belt. In the device, a wire is wrapped around

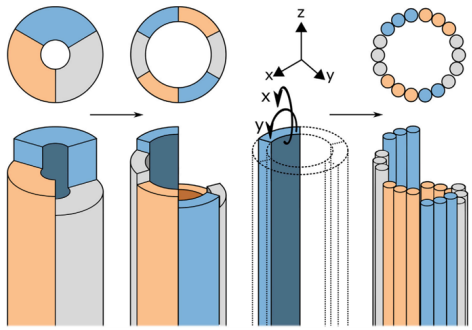

Fig. 4: Schematic representation of the friction-based flexible blade transportation device [6].

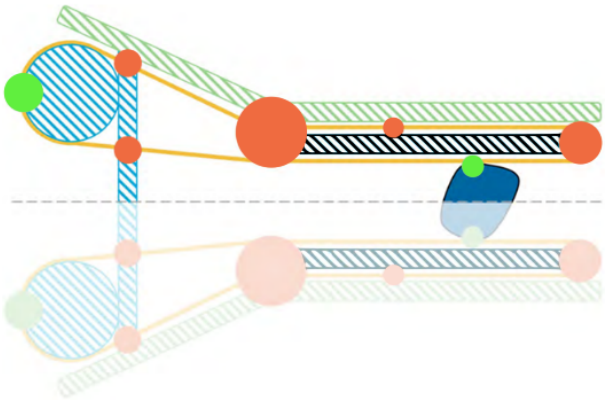

Fig. 5: Schematic overview of the friction-based rigid tissue transporting device. The green and orange dots resemble areas in which friction is either desired or not, respectively [11].

the wall of the tubular body (black), and over a gear (blue). When the gears are actuated, the wires start translating along the tubular body, pulling tissue into the device. The tissue is transported towards the cone, this is where the diameter of the device increases. The wires diverge and the tissue is released. All wires move into the same direction, taking full advantage of the generated friction force between the wires and the tissue. Appendix B contains more information on the device and its parts developed by Verberne et al. [11].

The tubular body is rigid as the device is dependent on constant wire tension. Constant tension keeps the wires into place and makes sure that the frictional interaction between the wires and gears remains steady. However, there is a trade-off for the amount of wire tension. For optimal performance of the transport mechanism, friction between the actuating gears and the wire is desired as more friction leads to a bigger driving force and less slippage. Friction between the wires and the tissue is also desired, to be able to transport the tissue at the same velocity as the wires. Friction at all other areas is undesired, as it leads to more resistance on wire movement and thus increases the necessary driving torque. Increasing tension on the wires results in higher friction forces at the gears, while also resulting in more undesired friction between the tip of the tubular body and the wires.

D. Comparison

Figure 6 shows a simplified schematic overview of standard suction catheters, the blade mechanisms developed by Sakes et al. [5] and De Kater et al. [6], and the wire mechanism developed by Verberne et al. [11]. The suction catheter cross section consists of a hollow shaft, the suction force exerts a force on the tissue in the shaft due to the pressure gradient between left and right. The suction force is distributed over the surface of the tissue, and pulls it into the direction of transportation. Friction occurs between the shaft walls and the tissue, resisting the motion in the transport direction. The cross section of the blade mechanism consists of six blades inside the hollow shaft. The schematic view has three blades for easier visualisation. Each blade exerts a push force at a point on the tissue, with most blades moving into the direction of transportation. The tissue has no contact with the shaft walls, but friction is generated by the blade that moves against the direction of transportation. The cross section of the wire mechanism consists of a hollow shaft with ten wires wrapped around it. Each wire translates along the shaft wall and generates a point force on the tissue, pushing it into the direction of transportation. Friction occurs between the tissue and the shaft walls, resisting motion into the direction of transportation.

Regarding the blade and wire mechanisms, the transportation rates are independent of the outer dimensions and the mechanisms are not prone to clogging as they use friction-based transport by utilising either blades or wires. The advantage of the mechanism developed by Verberne et al. [11] over both blade mechanisms is that all wires translate in the transport direction, rather than one in six blades moving against the direction of transport. The wire mechanism making more effective use of the generated friction showed in the achieved transportation rates of the different devices. The device developed by Sakes et al. [5] achieved a low transportation rate of 0.25 g/min, while the device of Verberne et al. [11] achieved a rate of 8.9 g/min, comparable to commercially available morcellators. The transportation rate of the device developed by De Kater et al. [6] was not evaluated. A big downside to the device developed by Verberne et al. [11] is that the shaft is not flexible, which restricts its use during Ear Nose and Throat (ENT) and cardiovascular applications.

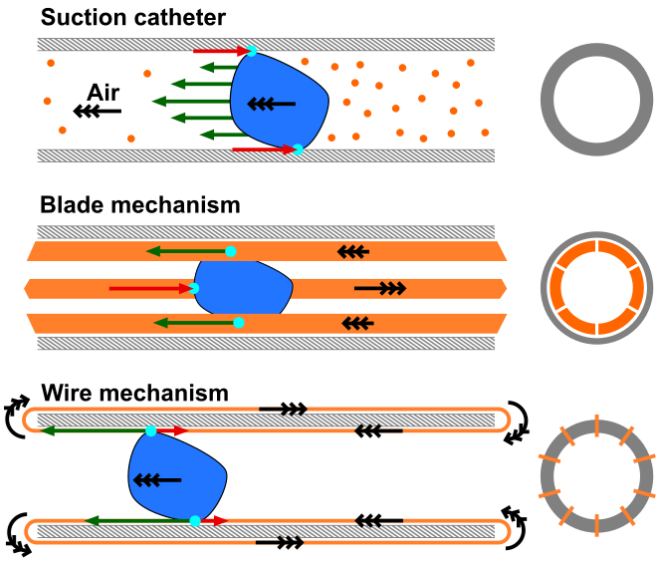

Fig. 6: Schematic overview of different transportation mechanisms with corresponding cross sections. Green arrows represent forces in the desired direction of transportation, red arrows friction forces, and black triple arrows direction of motion.

III. Design Problem Analysis

A. Design Requirements

The designed device must meet requirements for transportation functionality and for the procedure of MIS. All design wishes can be found in Appendix A. The requirements are as follows:

Transportation requirements

1) *Type of transportation:* The device enables continuous transportation of tissue
2) *Tissue elasticity:* The device enables transport of tissue with a Young's modulus range of 1-110 kPa [12] [13]
3) *Transportation efficiency:*The device enables a minimum transportation efficiency of 90%
4) *Reliability:* The reliability of the device is at least 90%
5) *Bendability:* The device enables tissue transportation within a curvature of 90 degrees over a shaft length of 80 mm [6] [14]

Procedure requirements

6) *Stiffness:* The stiffness of the shaft of the device should be between 598 and 791 Nmm^2 [15]
7) *Shaft diameter:* The device has a maximum outer and minimum inner diameter of 10 and 5 mm respectively
8) *Working length:* The device enables a minimum working length of 400 mm

1) Type of transportation: Continuous transportation was selected over discontinuous transportation due to its potential for higher efficiency and lower transportation time, both are critical in medical applications where precise and rapid tissue removal is desired. Continuous transportation provides uninterrupted movement to allow the tissue to be transported smoothly and consistently, ensuring that the friction between the wires and tissue remains steady. This reduces the risk of slippage and thus enhances the reliability of the device. Discontinuous transportation involves starts and stops, which lower the average transportation velocity and thus increase transportation time. Furthermore, discontinuous movement involves acceleration and deceleration of components. These changes in acceleration require larger forces than continuous movement of components, therefore resulting in higher wear.

Lowering the wear on components helps the device to maintain consistent performance during repeated use.

2) Tissue elasticity: The elasticity of tissue varies among different types of tissue and different diseases. For example, research on kidney tumours illustrated that the Young's modulus of kidney tumours is approximately 20 kPa higher compared to healthy tissue [16]. The selected range for tissue elasticity in this study is 1-110 kPa, which includes a wide variety of tissue properties that can be encountered during MIS (excluding bone tissue). The lower end of this range includes soft matter such as brain and adipose tissue with low strain rates (+ 1 kPa [12]). The higher end of this range includes stiffer matter such as tendons [13]. Aspiration-actuated devices are assumed to be suitable for the removal of fluids and liquids. Therefore, the transportation of liquids falls outside the scope of this study.

3) Transportation efficiency: The flow rates of ten tested commercially available aspiration catheters vary between 61.8 and 264.4 g/min [17]. These flow rates are achieved during transportation of liquids and are thus not representative for the removal of coherent tissue. Transportation rates of clinically available morcellators are more indicative, with rates varying between 6.2 to 40.4 g/min during laparoscopic surgery [18]. Regarding novel tissue transporting devices, both the rigid wasp-inspired friction transportation device by Sakes et al. [5] and the flexible wasp-inspired friction transportation device by De Kater et al. [6] reported their performance in transportation efficiency, values between 18 and 37% were achieved. In this study, the transportation performance will be denoted in transportation efficiency. The transportation efficiency is required to be at least 90 percent to show the potential of the device, and limit both slippage and damage of the transported tissue.

4) Reliability: Reliability is extremely important for medical instruments, as it has a vital impact on medical procedures. Reliability for the developed device is defined as the ratio between the ability to successfully transport tissue through the shaft of the device divided by the number of total transportation attempts. The reliability is desired to be minimum 90 percent, to indicate the potency of the device.

5) Bendability: Instruments used during laparoscopic surgery are rigid, while catheters consist of a flexible shaft that allows for bending around obstacles in the body. The smallest curvature a standard catheter can bend is 90 degrees [14]. In the study by De Kater et al. [6], the performance of the wasp-inspired tissue transporting device was tested at angles of 30 and 60 degrees, both over a shaft length of 80 mm. These curvatures had no statistical influence on the transportation rate of the tissue. In this study, the catheter bending angle is taken as a benchmark value, with the addition that this bending angle occurs over a shaft length of 80 mm, see Figure 7.

6) Stiffness: Bending stiffness is important for a flexible device. High bending stiffness can result in a device that is difficult to navigate through curves, and poses a high risk of tissue damage, while a low bending stiffness can cause difficulties when inserting the device, as it might deform

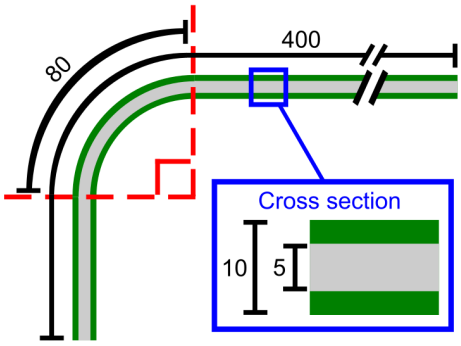

Fig. 7: Dimensional requirements for the shaft of the device, all lengths are in mm.

and get jammed into place. Research on proximal and distal catheter stiffness by Brandt-Wunderlich et al. [15] found a range of stiffnesses from 598 to 791 Nmm^2. These values were found by performing static bending tests, in which deformation occurred by applying a force to the clamped catheter. The proximal part of the catheter is stiffer as it guarantees pushability of the catheter, whilst the distal part allows for manoeuvrability. The range of stiffness for the shaft is chosen as 598 to 791 Nmm^2, this allows for sufficient stiffness for pushability of the shaft.

7) Shaft diameter: Diameters of aspiration-actuated catheters typically vary between 1 and 2 mm [17]. However, dimensions can be different depending on the medical procedure. For example, commonly used colonoscopes and morcellators have maximum diameters in the range of 13 to 20 mm [19] [18]. For this research, no strict size requirements were imposed, as to avoid the challenges of high manufacturing precision and assembly difficulties posed by smaller parts. Therefore, the shaft is required to have the following maximum outer diameter and minimum inner diameter: D_{outer} = 10 mm and D_{inner} = 5 mm.

8) Working length: Commonly used catheters enable a working length varying between 1.25 and 1.53 m [17]. Commercially available morcellators can have working lengths of around 420 mm [20]. A catheter is used to remove liquid matter, while a morcellator is used to remove solid tissue out of the body. As this study focuses on a device for transportation of solid tissue, it was decided that the developed device needs to have a minimum working length of 400 mm, a working length similar to a catheter is a wish as the device is then able to reach further into the human body.

B. Design Challenges

In this study, inspiration is taken from both De Kater et al. [6] and Verberne et al. [11] to design a friction-based flexible tissue transporting device. The device needs to have a flexible shaft, through which tissue is transported. Transportation will be done by translating wires, mimicking a conveyor belt. This transportation mechanism is chosen as previous work shows promising results. An abstract representation of the design

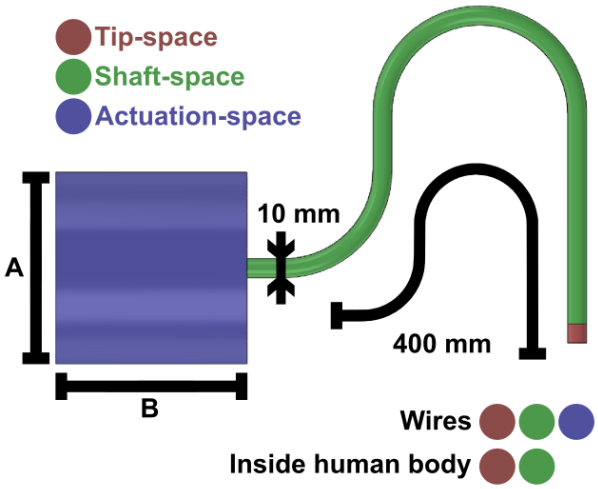

Fig. 8: Abstract representation of the design challenges. The tip-space is important for wire guidance, kink prevention, and minimisation of friction. The shaft-space guides the tissue and wires, and has to be flexible while complying with dimensional restrictions. The actuation-space has no dimensional restrictions, and needs to provide actuation to comply with the transportation requirements. The wires are part of the actuation system and pass through all three design spaces, the tip- and shaft-space enter the human body.

challenges can be seen in Figure 8. Three design spaces are present: 1) the pre-shaft or tip-space, 2) the shaft itself or shaft-space, and 3) the post-shaft or actuation-space (outside of the human body). Each design space has to fulfil different functions and has different restrictions, which can be linked to the design requirements in section III-A.

The tip-space has to comply with dimensional restrictions. The functions this design space needs to fulfil are wire guiding and kink prevention when the wire is guided from outside towards inside of the shaft. Friction needs to be minimised between the wire and these components to reduce both wear on the components and the necessary driving torque for the device as a whole. The tip-space is located at the far end of the device.

The shaft-space has to comply with requirements 2, 5-8. The shaft has to allow for transportation of a range of different tissues (R2), be able to bend 90 degrees (R5), have a stiffness within the specified range (R6), comply with dimensional restrictions (R7), and have a total minimum length (R8). The shaft-space is long and slender due to the dimensional requirements on its diameter. Tissue is guided through and wires are guided around and through the flexible shaft. High friction between wire and tissue is desired while the friction between wire and shaft wall should be minimised. The outside of the shaft should not contain any moving components (excluding the tip) to prevent unwanted tissue damage during operation.

The actuation-space has no dimensional restrictions and its main function is actuation of the device. It needs to comply with requirements 1, 3, and 4, providing continuous actuation (R1) for transportation at a minimum transportation efficiency (R3) with a high reliability (R4). Actuation power needs to be transmitted from a source to the wires, the wires must be guided from the actuation source to the shaft. Wires need to be separated in order to retrieve the transported tissue. As the shaft undergoes curvature, the effective length of the wires may vary. To make sure all wires stay into place, a mechanism should be present to regulate the effective length of each of the wires.

IV. Design and Prototype

A. Tip-space Design

From the design requirements and challenges discussed in section III-B, ideas were generated for possible concepts for each design space. Each tip concept should focus on wire guidance, kink prevention, and minimise friction. Two tip concepts can be seen in Figure 9. The left tip concept consists of a hollow ring and guides the wires by using cutout slots. The ring has a curvature from the outside to the inside to prevent kink and lower friction as the wire smoothly reverses direction. The right concept consists of a ring with roller bearings. The blue rollers have cutouts for wire guidance and prevent kink due to their roundness. The rollers generate low friction on the wires as there is no relative movement between the wires and rollers.

The concept with roller bearings has a higher potential for lower friction compared to the slotted tip concept, as no relative motion occurs between the wires and the rollers. This comes at the cost of a higher difficulty in manufacturing and assembly of the roller bearing concept. It has a higher part count than the single part slotted tip concept and needs assembly, which is difficult for the small scale required for MIS. Therefore, the roller bearing tip concept was deemed infeasible to manufacture. The final tip design was an improved version of the slotted concept, and can be seen in Figure 10. To ensure guiding of the wires with slots, the area in between the slots was raised 3 mm to prevent wires touching each other and

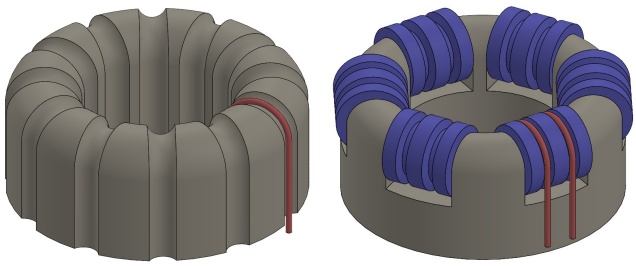

(a) Slotted tip concept. (b) Roller bearing tip concept.

Fig. 9: Tip concepts for wire guidance and kink prevention. The left concept uses a large curvature for smooth and low friction wire guidance, the right concept generates low friction as there is no relative motion between the wires and rollers.

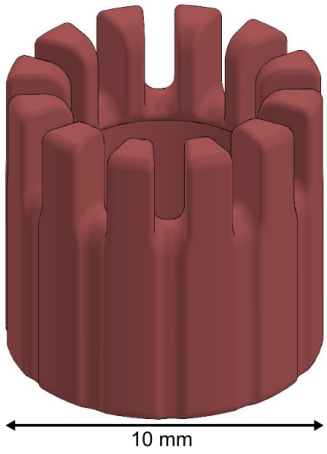

Fig. 10: Final tip design for the prototype.

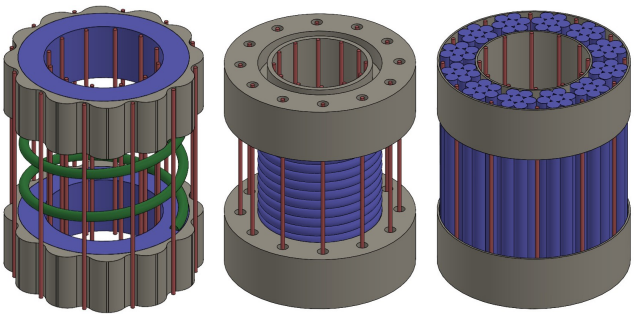

(a) Magnet rings. (b) Slotted rings. (c) Stationary cables.

Fig. 11: Three flexible shaft concepts with moving wires in red. The left concept guides the wires using magnetic force and is flexible due to the compression spring. The middle concept guides wires through holes and is flexible due to the tension spring. The right concept guides the wires through gaps between cables, the cables provide flexibility.

leaving the slots. The slots are 1 mm wide and the total height of the part is 9.6 mm.

B. Shaft-space Design

Each shaft concept should be flexible, guide the wires on the in and outside and minimise friction. Figure 11a shows a shaft concept using magnetic rings (blue), a compression spring (green), and magnet covers (grey). The compression spring provides flexibility, both ends are ground flat and attracted by the magnet rings. The magnet covers have grooves for wire guidance and are clamped onto the magnet rings. The ring magnets attract the wires by magnetic force, such that they stay in place. A second concept was designed using slotted rings (grey) and a tension spring (blue); it can be seen in Figure 11b. The spring is clamped into the round slot of the ring and allows for bending motion. The wires are guided through the small holes in the ring. A third concept using cables (blue) can be seen in Figure 11c. Bundles of flexible cables connect the thin inside and outside walls and provide flexibility. Wires are guided through gaps in between the cables, they translate on the inside of the inner wall and against the inside of the outer wall. In all three concepts, wires are not changing direction as that would increase the number of contact points with the shaft and thus friction.

Regarding manufacturability, the concept using magnet rings was infeasible. The available small size magnet rings on the market had too small inner diameters to satisfy the design requirements. The slotted ring concept was chosen over the concept with cables, as it involves less parts, and is easier to adapt to future changes in design. Changes to the slotted rings can be made easily, adding or removing holes and cuts while the cables offer little opportunity for modification. The final shaft-space design consisted of connection rings and a tension spring was clamped into the ring as can be seen in Figure 12. Regarding the connection rings, a long clamping distance would be beneficial for a more firm press fit and better alignment between ring and spring, while a shorter ring length would result in a shorter rigid section of the shaft. A clamping length of 6 mm was used, a shorter length resulted in an unstable connection between the spring and the ring. The connection ring clamps a spring on each side, and has a middle wall with a thickness of 2 mm, resulting in a total length of 14 mm.

A closed tension spring was selected for the final design, as it offers better guidance to tissue on the inside compared to an open spring and it is more stable. The spring has an inner and outer diameter of 6.1 and 8.6 mm respectively. The inner diameter of the ring is equal to the inner diameter of the spring, to prevent tissue from getting stuck on an edge between the spring and connection ring. As strict guidance is necessary during bending of the shaft, wires are guided through holes in the ring. Each wire has a knot for connecting the two ends, this knot is thicker than the wire itself. Therefore, the holes in the ring were maximised while complying the minimum wall thickness to make the knots slide through them easily. For extra guidance of the wires, additional add-on rings were 3D-printed and clamped onto the tension spring. These add-on rings are 7 mm thick and consist of two parts that fit into each other, such that they can be added and removed from the spring. Both the connection ring and add-on ring were designed to have a maximum outer diameter of 10 mm, but the parts ended up with a 15 mm diameter due to limitations of the manufacturing process. More on this in section IV-D2.

C. Actuation-space Design

It is important for actuation concepts to behave continuously, guide the wires, generate force to move the wires, and regulate the tension on the wires. These requirements were split into two, concepts for wire guidance and continuous force generation, and concepts for tension regulation. Continuous actuation resulted in all concepts making use of rotating wheels and gears. Every driving concept should generate grip between the wheel/gear and the wire, four concepts were generated with different working principles, and can be seen in

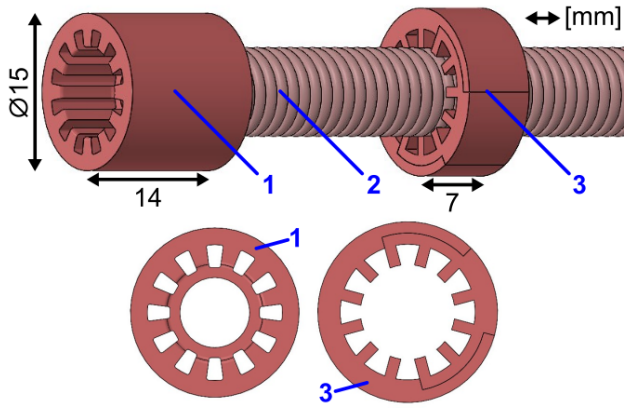

Fig. 12: Connection ring (1), spring (2), and add-on ring (3).

Figure 13. Two concepts increase grip by increasing normal force on the wire (a, b), and two concepts increase grip by shape (c, d).

Figure 13a shows a concept design with two wheels squeezing the wire together. The concave wheel is guiding the wire, while the convex wheel is pushed onto the concave wheel to increase normal force and grip. A concept using magnetic force is shown in Figure 13b, the wheel has a (blue) magnetic core and an outside ring with a small cutout (grey). The outside ring is clamped onto the magnetic core and guides the wire, the magnetic core attracts the wire to the wheel to increase normal force and grip. In Figure 13c, a concept with wire shape-gripping is shown. The gear wheel has teeth with a cutout and the wire has a variable diameter, this can be due to knots in the wire. The teeth cutouts guide the wire, the thin section of the wire can pass through the cutout while the thicker section cannot. Figure 13d shows a concept with two gears with round teeth, which grip into each other but also grip the wire. Both gears rotate and push the wire forward. This shape-grip does not require a wire with a variable diameter, but it requires two gears instead of one.

Two concepts were created to regulate tension, one regulates tension passively while the other concept can be adjusted manually. A concept inspired by a bicycle chain tensioner can be seen in Figure 14a. This concept has an element with a compression spring (blue), the spring pushes on the wire to create tension. If the wire slacks, the spring elongates until the wire tension finds a new balance with the spring force. The tension is regulated passively and the concept is not adjustable. Figure 14b shows a concept with a thread (blue), nut (green), and guiding axis (blue). By turning the nut, the platform will move up or down over the thread and smooth axis to increase or decrease the wire tension. This way, the wire tension can be adjusted manually.

The actuation for the device was designed to consist of six similar small actuation units that each actuate two wires. Each wire would ideally have its own actuation unit, but this would result in the device becoming too large. Twelve wires in total translate along the shaft, and were deemed enough to transport

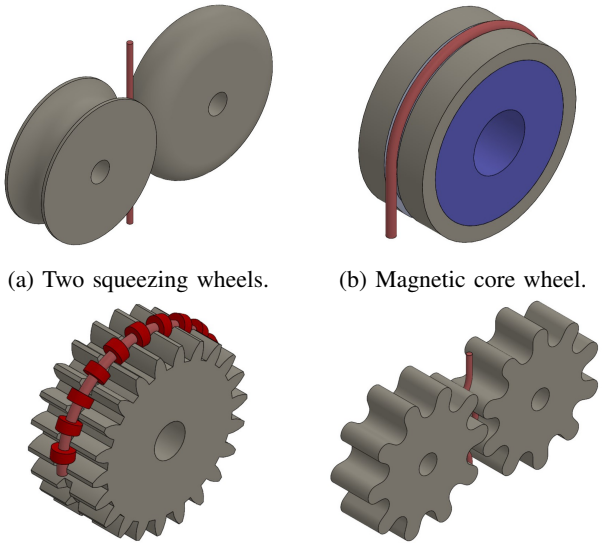

(a) Two squeezing wheels. (b) Magnetic core wheel.

(c) Wire grip gear. (d) Two gripping gears.

Fig. 13: Different concepts for creating driving friction. Concepts (a, b) increase grip by increasing normal force on the wire, concepts (c, d) increase grip by shape.

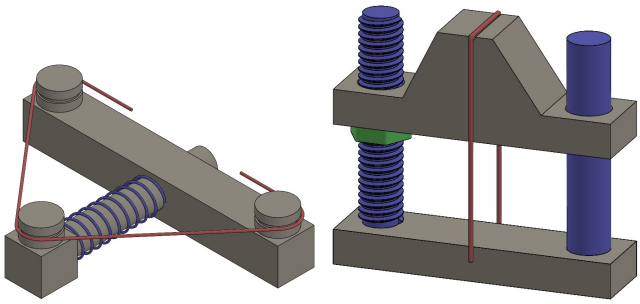

(a) Sprung element. (b) Adjustable guided platform.

Fig. 14: Two concepts for achieving constant wire tension. The left concept regulates wire tension passively using a compression spring, the right concept is to regulate tension manually by adjusting the screw.

the tissue and prevent it from touching the stationary shaft, which would lead to increased friction.

Regarding feasibility for the gear and wheel concepts, the magnetic core wheel was dropped due to complexity and low availability of small magnets. The wire grip gear was undesired as it needed an adaptation to the wire, which made wire guidance difficult. Both the two squeezing wheels and the two gripping gears were manufactured and tested to compare their performance as both designs seemed promising. The two gripping gears yielded greater friction and offered lower complexity, as the use of a spring was unnecessary unlike the two squeezing wheels.

The final single actuation unit can be seen in Figure 15. Three gears are present, a bevel-spur gear with larger teeth (1), a bevel-spur gear with smaller teeth (2), and a spur gear

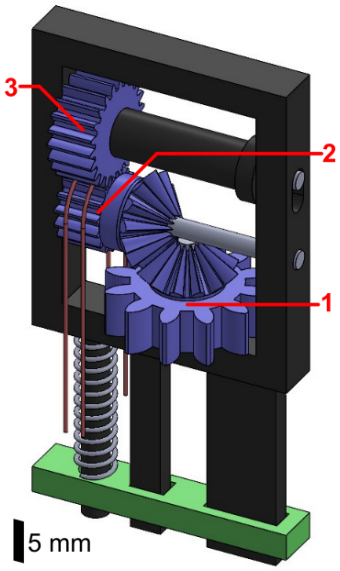

Fig. 15: Actuation unit consisting of two bevel-spur gears (1, 2) and one spur gear (3) with tension regulating mechanism.

(3). The bottom gear is driven and oriented horizontally, such that all actuation units have the same plane of actuation. As the wires need to travel the shaft in axial direction, the second gear is rotated 90 degrees from the first gear. The bevel heads of both gears transmit the power over 90 degrees. The power is then transmitted from spur to spur gear such that the third gear also rotates. The wire is gripped in between the second and third gears and pushed forward. The third gear has linear guidance to be able to move vertically slightly, as the wire has a knot to connect both ends and this knot is thicker than the wire itself. All three gears are fitted onto axes in a square 29.5 x 5.2 x 35.5 mm frame. The axes for the first and second gears are press fitted into the frame, while the top axis can slide vertically into the slotted hole. The top axis is held in place as the black aligner part is press fitted onto the axis.

To regulate the tension of the wire with variable length, a combination of the two concepts shown in Figure 14 was used. It is important that the tension is regulated passively to limit the amount of actions during operation of the device. The green rectangular prism in the bottom of Figure 15 represents the part that the actuation unit is attached to. The square frame has three guiding rods, one circular and two rectangular. The circular guiding rod is to prevent the spring from buckling, the other two provide stability. The circular guiding rod is placed below the bevel-spur gear to have the tension and spring forces in the same line of action, this will prevent any net moment force. The spring mechanism regulates the tension in the wire passively, an increase in wire tension will yield compression of the spring until a new balance of forces is obtained.

D. Final Prototype

1) Integration: To combine the solutions for the different design spaces, other parts had to be designed to connect everything. The shaft is long and slender due to dimensional restrictions, but the actuation-space of the device has a larger diameter. To transition from the smaller to larger diameter, a cone-shaped part was designed. The cone is shown in orange in Figure 16. The shaft is press fitted into the small end of the cone using the same principle as the connection ring. The big end is circular with a square cutout, this is to connect the actuation base to the cone and prevent relative rotation between the two parts. The small end of the cone guides the wires and due to the diameter change, the wires diverge, and the tissue can be extracted. To allow for tissue removal, the middle part of the cone consists of three spokes with large space in between for accessibility. The outside of the cone has a thread to fit a ring that can be screwed onto it. This tension ring can be seen in yellow in Figure 16 and 17. By screwing the tension ring up or down, the distance between the cone and the actuation base can be adjusted. It is important to be able to adjust the wire tension for the functionality of the device, too high tension will result in high friction and too low tension might result in wires not being guided correctly along the device.

The actuation base is where all actuation units are attached to. It has two different diameters, such that the drive ring can fit onto it as can be seen in Figure 16. The drive ring has to transmit power from outside to the gears, while also shielding the actuation units from the outside of the device. The drive ring has 120 markers on the outside to be able to measure its rotation, which is necessary to determine the rotation of the gears and the translation of the wires. The bottom of the actuation base has a C-shaped slot to fit onto the cone, the top part can be seen in Figure 18. In this Figure, a circular pattern of six rectangles (1) shows where each of the six actuation unit frames will be placed. Each actuation unit has guiding pins that will slide vertically into the one circular and two rectangular holes (2). Two holes with rounded ends (3) will guide two wires from the cone and bottom of the actuation base to each actuation unit. Six rectangular cutouts (4) are present on the inside of the base, these are to press fit the cover. The cover closes the actuation from the top and keeps the drive ring into place (Figure 16). The assembled design can be seen in Figure 19, all parts of this design in different views can be seen in Figure 35 in Appendix C.

2) Manufacturing and optimisation : Figure 19 shows the final manufactured prototype. It was chosen to use additive manufacturing to create the final prototype due to ease of use, ease to make changes to parts, speed of manufacturing and the ability to produce everything in-house. Two types of printers were available: two FDM 3D-printers (Prusa MK3S, Ultimaker S5) and with lower availability a SLA 3D-printer (Formlabs 3B). The tip part was manufactured with SLA printing (Tough resin), as curves and edges were very small and needed to be smooth for guiding of the wires. All other parts were designed for FDM 3D-printing with PLA. Three parts had to be increased in size due to restrictions of the manufacturing process. The connection ring, add-on ring and cone needed adaptations due to resolution (0.3 mm), minimum

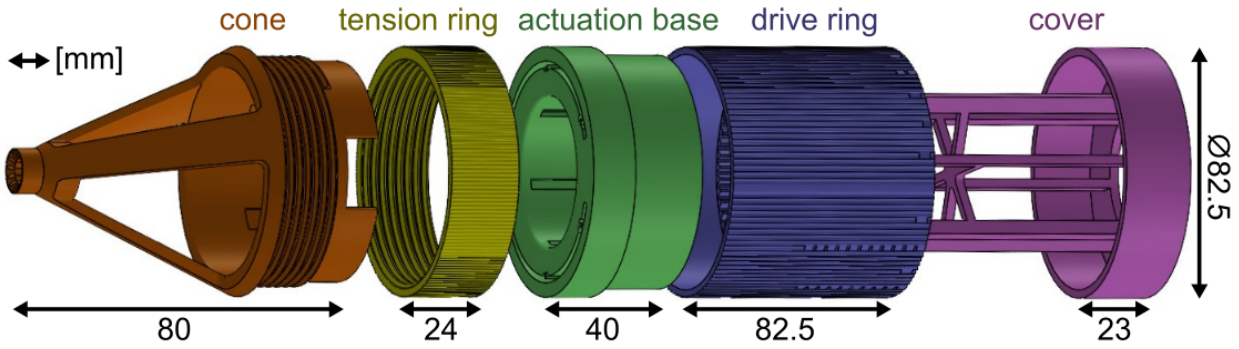

Fig. 16: Left to right: cone, tension ring, actuation base, drive ring, and cover.

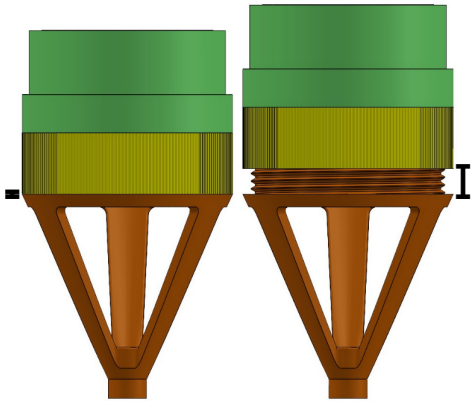

Fig. 17: Variable distance between cone and actuation base.

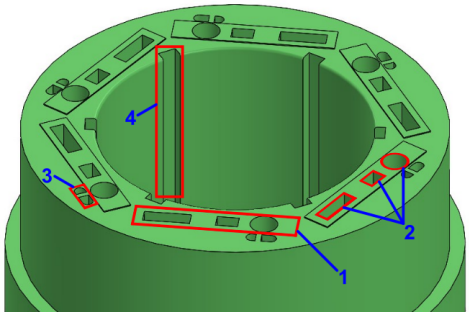

Fig. 18: Top view of the actuation base with placement of six actuation units (1), holes for guiding pins (2), holes for wire guidance (3), and cutouts for the cover (4).

wall thickness (1 mm), and minimum hole size (0.5 mm) associated with FDM printing. Figure 20 shows the rings of the final design on the top and the rings for the prototype on the bottom. The add-on ring consists of two parts that both need to be 1 mm thick and therefore the outside wall is two times 1 mm thick. This and the other changes resulted in the rings having a diameter of 15 mm instead of 10 mm. The cone tip cross section was changed according to the connection ring as it fulfils the same functions of wire guiding and clamping the tension spring.

An important challenge to tackle was the flow through the shaft, the translation of the tissue on the inside and the wires on both sides of the shaft. Different iterations of the connection ring can be seen in Figure 21. At first, the spring was clamped from the inside and outside as seen in the most left ring in the figure, resulting in a sturdy connection. This also meant that the inner diameter of the ring was smaller than the inner diameter of the spring. Due to this difference in diameter, tissue kept getting stuck on the little edge of the connection ring. The middle ring in the picture has the middle section removed, having the same inner diameter as the spring. As the spring is now only clamped from the outside, it is clamped over a longer distance to ensure a sturdy connection. The ring on the right has bigger holes compared to the middle ring, to ensure smooth guidance of the wires and knots. Each wire loop from actuation unit to the tip consists of one wire with both ends tied together by a knot. This knot is thicker than the wire itself, which led to the knots getting stuck in the guidance holes. The holes in the right ring were maximised, while respecting the dimensional restrictions for MIS and respecting the minimum wall thickness for FDM 3D-printing. Besides this, the size of the knots was minimised. Fishing line 0.22 mm thick is used for the wires. As the fishing line has very low friction on itself, most available knots consisted of a large number of wraps and twists which resulted in a very thick or long knot. The best option found was a square knot, a knot which is relatively flat, and has a small knot in both ends to prevent the knot from getting loose. It can be seen in Figure 40, in Appendix D.

The cone guides and separates the wires from each other due to increasing diameter. The thin end of the cone uses the same principle as the connection ring to clamp the shaft. Instead of a flat surface, the surface has an angle inward for guidance of the knots. As the wires diverge, they are sliding against the outside of the cone tip. A flat surface would not guide the knots well as they get stuck on the outer edge sometimes, an angled surface makes the knots slide into the holes more reliably. On the bottom of the cone, six slots are cut. This was needed to split the slotted holes for guiding the wires in the Actuation base into two holes, this can be seen in Figure 18 hole number three. The separation runs from the bottom to the top of the actuation base, the separation is placed such that

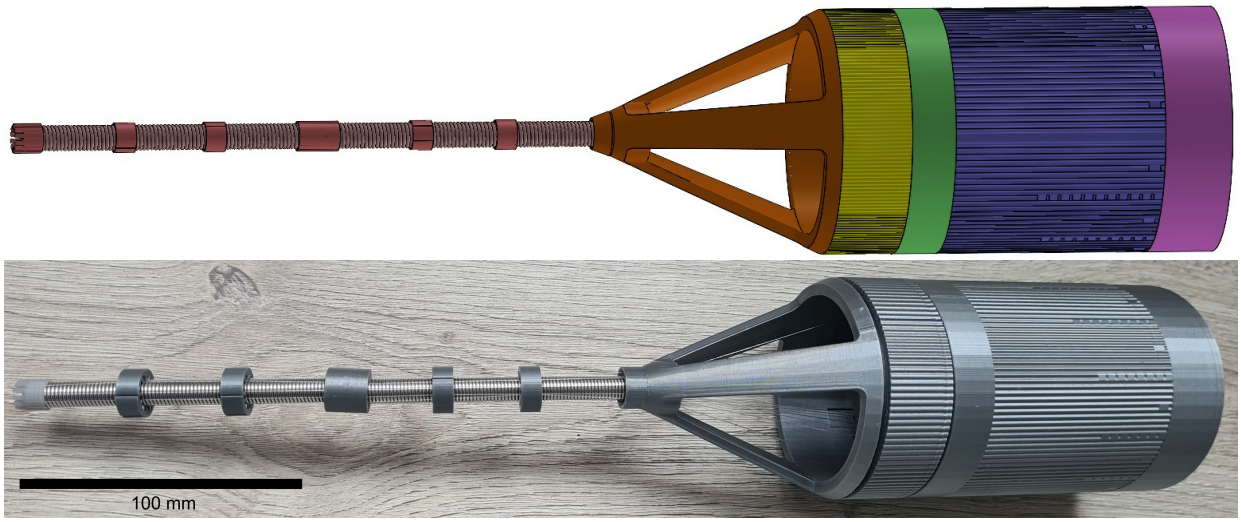

Fig. 19: Final design versus final prototype with a 20 cm shaft.

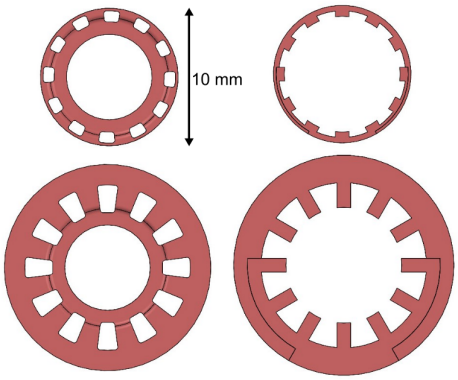

Fig. 20: Connection and add-on rings of final design versus prototype design due to manufacturing restrictions.

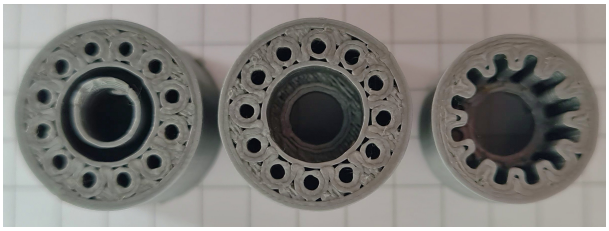

Fig. 21: Different iterations of the connection ring.

both openings on the bottom of the actuation base have the same size. Figure 22 shows different iterations of the actuation base, the holes for the springs were increased, the cutouts for the cover were changed, and the width of the holes for the actuation unit pins were increased. On the right, the part with the separation in the slotted hole can be seen. The final part for guiding the wires is located on the actuation units. This guide is a small extrude with two slotted holes, best visible in Appendix C, in Figure 35g.

The second challenge in guiding the wire is achieving

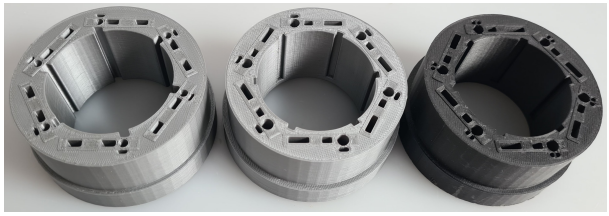

Fig. 22: Different iterations of the actuation base.

constant wire tension. When the effective length of a wire changes, the tension in a wire changes as well. The tension will be regulated for the device as a whole and for each actuation unit independently. By screwing the tension ring up or down, the tension on all wires can be in- or decreased. A second mechanism is located below each individual actuation unit, which can regulate the tension over two wires. The actuation unit frame has three guiding pins which can slide vertically through the actuation base. After some testing, it was found that 25 mm of vertical adjustment was desirable, to account for extreme curvature of the shaft of 360 degrees (one full rotation). As this would significantly increase the height of the actuation base and drive ring, the pin holes were integrated through the actuation base. The circular cutout in the actuation base has two different diameters, first: to allow the spring and pin to fit into it and, second: a smaller hole that only the guiding pin will fit through. The holes for the other two square pins are cut through the whole actuation base except 1 millimetre, this was necessary for the manufacturing process as the print failed to generate accurate holes otherwise. The pin shape and size was increased until each actuation unit would move smooth and only vertically.

Significant changes were made to the actuation units. Most important were the alterations to the gears and wheels. Each version consists of a frame and three gears, multiple gears and wheels are shown in Figure 23. The bevel-spur with larger

teeth (bottom) transmits the power from the drive ring to the rest of the gears and did not undergo any changes, changes were made to the two wheels that drive the wire. The left set of three shows rounded wheels that push into each other to create friction on the wire. The two top wheels need a spring force to push them against each other, this concept did not generate sufficient friction. The wheels in the middle set have teeth to grip the wire to generate friction without a spring force. The middle gear of the set has two higher walls to prevent the wire from sliding off the teeth. This concept generates sufficient friction, but the walls of the bevel-spur gear seemed unnecessary. As the wires were guided on both sides of the gear, they did not slip to another position. Therefore, the walls were removed, and the three gears on the right were the final gears to be used for the prototype. All gears were FDM printed, as this was sufficient for the parts to rotate and grip into each other.

V. Experimental Validation

A. Goal

As stated in section I-C, the goal of this study is to design a flexible friction-based continuous tissue transporting device compatible with MIS in which the transportation efficiency is independent of tissue elasticity within the Young's modulus range of 1-110 kPa. This goal is related to the performance of the device, which can be tested through experimental validation of the prototype. Three sets of experiments were designed to evaluate the influence of four variables on the transportation efficiency, set 1 investigating the tissue elasticity and shape, set 2 the shaft curvature, and set 3 the device orientation.

B. Experiment Independent Variables

1) Tissue elasticity and shape: The designed transportation mechanism should be able to transport tissues within the elasticity range of 1-110 kPa, this includes a wide variety of tissues that can be encountered during MIS. To replicate the mechanical properties corresponding to the specified elasticity range, tissue phantoms were created using a combination of water and gelatin. The prepared phantoms contain gelatin weight percentages of 3, 9, and 12, which correspond to estimated elasticity values of 1-10, 55, and 100-110 kPa respectively [21]. It is important to note that the referenced study does not provide explicit data for the extremities. Therefore, the corresponding Young's moduli are estimations. To enhance visibility of the phantoms during experiments, red food colouring is added. Transportation is facilitated by the friction between the wires and the tissue. The wires are distributed uniformly along the inside of the shaft. When the cross section of the shaft is entirely filled with tissue, all wires contribute to the transportation of the tissue. If the tissue is not filling the entire cross section, a reduced number of wires contribute to the transportation of the tissue. To evaluate the influence of this effect, experiments are conducted using both cylindrical and half-cylindrical tissue phantoms. Each phantom has a diameter of 5 and height of 15 millimetres respectively.

2) Curvature: The tubular structure of the device is flexible such that it can navigate the human body and reach the desired position for tissue removal. Different curvatures allow the device to manoeuvre through complex anatomical pathways effectively. Figure 24 shows a part of the shaft in a bending angle of 90 degrees. A greater degree of curvature may impact the contact areas between the tissue, tubular wall, and wires, potentially affecting the transportation efficiency. In the experiments, the tubular curvature is adjusted from 0 to 90 degrees in increments of 30 degrees to evaluate its influence on the transportation efficiency and reliability. Besides these scenarios, the extreme scenario of a 180 degree S-curve is also investigated.

3) Orientation: During MIS, the tubular structure consisting of the shaft and tip of the device is advanced within the human body until the position for tissue removal is reached. The orientation of the tubular structure is adjusted incrementally to cause the least damage to surrounding tissue when manoeuvring from the incision to the desired position. Adjusting the orientation will alter the effect of gravity on the tissue in the tubular structure. For instance, the gravitational force will oppose the direction of transportation when the tubular structure is oriented with its tip facing downward. When the

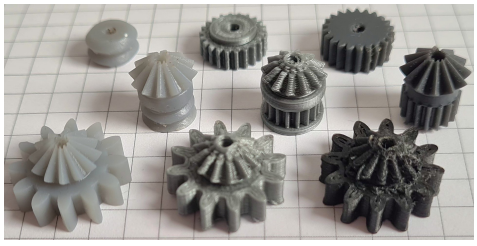

Fig. 23: Different iterations of gears and wheels.

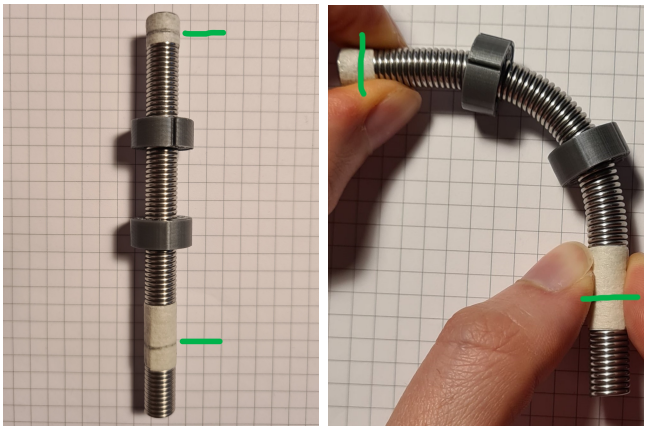

(a) Straight shaft section. (b) shaft section bent 90 degrees.

Fig. 24: A part of the shaft in a 90 degree bending angle. The distance between the two marked ends is 80 mm.

tip of the tubular structure is facing upward, the gravitational force will comply with the direction of transportation. The orientation of the tubular structure in the experiment setup can be varied from minus 90 degrees (tip facing downward) to plus 90 degrees (tip facing upward) in increments of 45 degrees.

C. Experiment Dependent Variables

1) Transportation distance: The developed mechanism is driven by the rotation of the drive ring, not visible in Figure 15. The motion of the drive ring will transfer from the bottom bevel-spur gear (1) of each actuation unit to the second bevel-spur gear (2) and top spur gear (3), and results in linear translation of the wire. All transmissions are assumed to be ideal and have no slip. The drive ring and gears of the actuation units have a set number of teeth, such that their rotations are all relative to one another. The rotation of the drive ring in degrees generates a certain wire and thus tissue transportation distance in millimetres. This transportation distance is calculated according to Equation 2. The transportation distance is indicated by d_{wire}, $N_{markers}$ indicates the amount of markers that the drive ring has rotated, this is divided by 120 as the drive ring has 120 markers for a full rotation, $teeth_{DR}$ is the number of teeth on the drive ring, $teeth_{gear1}$ the number of teeth on the first gear of the actuation unit, and $\pi * D_{gear2}$ the circumference of the second gear of the actuation unit over which the wire passes.

$$d_{wire} = \frac{N_{markers}}{120} \cdot \frac{teeth_{DR}}{teeth_{gear1}} \cdot \pi \cdot D_{gear2} \tag{2}$$

Increasing the rotational velocity of the drive ring increases the rotational velocity of the gears in the actuation units and the wire transportation speed. However, excessive rotational speeds may induce slippage between the wires and tissue, which will result in the wires travelling a distance larger than the shaft length before the tissue exits the shaft. During all experiments, the drive ring is rotated manually with a slow and consistent velocity as this is hypothesised to generate the lowest slippage.

2) Transportation efficiency: Transportation efficiency is the ratio between the travelled distance of the wires and the shaft length. In an ideal scenario with no slip, both these distances are equal (100 %). Slippage can occur due to limited contact points between the wires and tissue, friction between the tissue and the tubular wall, or gravitational forces opposing the direction of transportation. The transportation efficiency is calculated according to Equation 3, $\eta_{transportation}$ being the transportation efficiency, l_{shaft} the shaft length, and d_{wire} the transportation distance.

$$\eta_{transportation} = \frac{l_{shaft}}{d_{wire}} \tag{3}$$

3) Transportation reliability: The transportation reliability reflects the success rate of transporting all tissue phantoms during the experiments. Issues like clogging or malfunctioning are unacceptable during medical procedures, therefore the goal is to maximise the reliability to ensure dependable performance. An attempt can be either a success or failure, the reliability is expressed as a percentage and calculated using Equation 4. Transportation reliability is indicated by r, the amount of failed and successful attempts by $N_{failure}$ and $N_{success}$ respectively.

$$r = \frac{N_{success}}{N_{failure} + N_{success}} \cdot 100 \tag{4}$$

D. Experiment Setup

The prototype was mounted onto a Thorlabs® plate for experiments, this plate consists of twenty-four times six M6 sized holes spaced 12.5 mm from each other core to core. The setup can be seen in Figure 25: it consists of the prototype, two circular plates with round and square holes (1), three supports (2), and three half round clamps (3). All parts necessary for the setup were manufactured using FDM 3D-printing. The prototype is supported under the actuation base, cone end, and the tip. Each of the three parts of the prototype is clamped by the support and a half circular clamp, which are bolted onto each other by M6 bolts and nuts. Both circular plates are bolted into the Thorlabs® plate to prevent the prototype from moving during experiments. The distance between the supports under the cone end and under the tip can be altered by using the square spacing holes, this is necessary for when the shaft changes length during curvature. To change the angle between the cone end and the tip, both supports can be rotated by using the circular holes in each circular plate. The circular plates have twenty-four holes, changing one hole will change the alignment by 15 degrees. When both circular plates change one hole, the curvature of the shaft will be 30 degrees. Figure 25 shows the shaft during 60 degree bending. To change the orientation of the prototype, a different setup was used, which is visualised in Figure 26. Two L-shaped supports (1) and two different clamps were manufactured. The prototype is clamped onto the actuation base by two hexagonal clamps that are mounted together (2), these two clamps form an octagonal shape on the outside of the prototype (3). The support and support clamp are mounted together and lock around the octagonal shape. The support clamp is removed in Figure 26 to show the octagonal shape. When dismounting the support and support clamp, the octagonal shape can be rotated by 45 degrees to change the orientation of the prototype.

The tension ring is stationary during experiments, and marked with a blue line to be able to measure the relative rotation of the drive ring. Before every experiment measurement, the drive ring is aligned with the tension ring. Tissue phantoms with 3, 9, and 12 weight% were prepared by creating multiple mixtures, pouring these into moulds, and refrigerating those for twelve to twenty-four hours. After solidifying, the solid sheets were cut to shape with a cutting tool. This resulted in each cylindrical phantom having a diameter and length of 5 and 15 mm respectively. Each phantom is used only once during experiments to prevent effects of wear and shape change

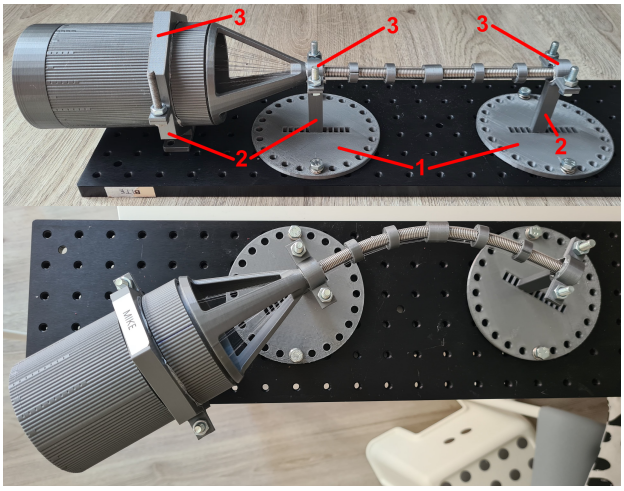

Fig. 25: Experiment setup on Thorlabs® plate consisting of circular plates (1), supports (2), and support clamps (3). Images during straight and 60 degree curvature positions.

Fig. 26: Experiment setup for different orientations of the prototype, consisting of two L-shaped supports (1), two hexagonal clamps (2), and an octagonal shape for orientation change (3).

when undergoing transportation. The cylindrical phantoms are split in half to create the half-cylindrical phantoms.

E. Experiment Protocol

Experiments were conducted on the prototype to evaluate the influence of tissue elasticity and shape, shaft curvature, and device orientation on the transportation efficiency. This resulted in fourteen experiments with variable conditions, divided into three experiment sets. Table I shows the different experiment conditions, each experiment is performed with five tissue phantoms. Experiment set 1 focuses on the influence of tissue properties on the transportation efficiency, set 2 focuses on the effect of curvature, and set 3 is to investigate the effect of orientation. Each experiment is conducted as follows. The prototype is mounted to the Thorlabs® plate using the manufactured supports and clamps. The drive ring is then aligned with the blue line on the tension ring, this is the zero position. Subsequently, the tissue phantom is inserted into the tip of the prototype. The drive ring can then be rotated and the wires will translate, transporting the phantom. The measurement is terminated when the tissue phantom has travelled the length of the shaft and is visible at the thin end of the cone. The phantom is then removed, this process is repeated five times for each combination of experimental variables.

F. Data Analysis

The experiments will yield values for the rotation of the drive ring relative to the stationary tension ring. The transportation distance of the wires for each combination of experiment conditions is calculated from the rotation of the drive ring with Equation 2. The shaft length is divided by the transportation distance, this results in the transportation efficiency. The shaft length for the straight configuration is 215 mm, bending of the shaft has a negligible effect on the total length. Per experiment set, scatter plots will be created from the derived transportation efficiency values, and a one-way Analysis of Variance (ANOVA) test will be performed for statistical validation. For the ANOVA test, it is hypothesised that the means of the groups within the different experiment set are equal. If the ANOVA test yields a significant result, this hypothesis is invalid. This indicates that the transportation efficiency is affected by the combination of experimental conditions in the concerning experiment set.

G. Results

All data extracted from the experiments is shown in Table I, some snapshots taken during experiments can be found in Appendix E. During 70 measurements, the prototype was unable to transport the tissue phantom 13 times. This resulted in the transportation reliability being 81%. Including the measurements of zero transportation, an average transportation efficiency of 75% was achieved for all experiment conditions. Figure 27 displays the influence of tissue properties on the transportation efficiency. The hollow circles denote the measurements with half-cylindrical tissue phantoms, the bold circles denote the measurements with cylindrical phantoms. Figure 28 shows the relation between prototype curvature and efficiency. The graph shows a reduced number of circles compared to the other experiment sets as the prototype was unable to transport the tissue phantoms during certain experiments. These measurements are not visible in the graph. Figure 29 shows the influence of device orientation on transportation

TABLE I: Experimental Protocol and Results

Experiment	**1.1**	**1.2**	**1.3**	**1.4**	**1.5**	**1.6**	**2.1**	**2.2**	**2.3**	**2.4**	**3.1**	**3.2**	**3.3**	**3.4**
Phantom (wt%)	3	3	9	9	12	12	12	12	12	12	12	12	12	12
Phantom shape	●	◒	●	◒	●	◒	●	●	●	●	●	●	●	●
Curvature (deg)	0	0	0	0	0	0	30	60	90	180	0	0	0	0
Orientation (deg)	0	0	0	0	0	0	0	0	0	0	-90	-45	45	90
η measurement 1	0.85	0.79	0.80	0.85	0.94	0.80	0.76	-	-	-	0.95	0.81	0.87	0.95
η measurement 2	0.95	0.80	0.86	0.98	0.94	0.81	0.77	-	-	-	0.95	0.90	0.92	0.98
η measurement 3	0.99	0.90	0.91	0.98	0.94	0.94	0.84	-	-	-	0.97	0.91	0.95	0.99
η measurement 4	1.00	0.97	0.99	0.98	0.96	0.94	0.87	-	-	-	0.98	0.98	0.96	0.99
η measurement 5	1.00	0.98	1.00	0.99	0.99	1.00	0.94	0.62	0.73	-	0.98	1.00	0.98	1.00
Average η	0.96	0.89	0.91	0.96	0.95	0.90	0.84	0.12	0.15	-	0.97	0.92	0.93	0.98
Reliability	100%	100%	100%	100%	100%	100%	100%	20%	20%	0%	100%	100%	100%	100%

Fig. 27: Scatter plot displaying the influence of tissue properties on transportation efficiency. Measurements for the half-cylindrical phantoms are denoted by hollow circles, the cylindrical phantoms are denoted by full circles. Overlapping measurements are shown as multicoloured circles.

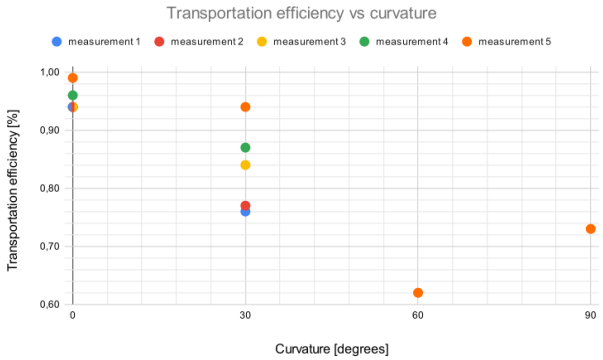

Fig. 28: Scatter plot displaying the influence of shaft curvature on transportation efficiency. Overlapping measurements are shown as multicoloured circles.

efficiency. Measurement 1 (blue) shows the lowest efficiency value per combination of experiment conditions, measurement 3 (yellow) is the median, and measurement 5 (orange) the highest value. For the ANOVA test, the null hypothesis was formulated as all group means within an experiment set being equal: $H_0 : \mu_1 = \mu_2 = \mu_k$, μ is the group mean, and k number of groups. Experiment set 1 had six groups, set 2 had four groups, and set 3 had five groups. The results of the one-way ANOVA test yielded [F(4,20) = 0.8674, p=0.50046] for set 1, [F(3,16) = 20.5768, p=0.00001] for set 2, and [F(4,20) = 1.7371, p=0.18140] for set 3. All tests were done at significance level p = 0.05. The results for set 1 and 3 were not significant, indicating that the transportation efficiency is independent of the tissue properties and device orientation. The results for set 2 were significant, indicating that the transportation efficiency is dependent on shaft curvature.

VI. Discussion

A. Main Findings

The goal of this study was to design a flexible friction-based continuous tissue transporting device compatible with MIS in which the transportation efficiency is independent of tissue elasticity within the Young's modulus range of 1-110 kPa. The design and procedure requirements (section III-A) and design wishes (Appendix section A) are evaluated to determine whether the prototype achieved its goals. The prototype successfully enabled continuous transportation of tissue through rotation of gears. The rotation of the gears resulted in translation of the wires, friction between the wires and tissue generated a smooth motion of the tissue through the shaft. The prototype was able to effectively transport tissues with two different shapes and various elasticity levels within the specified elasticity range of 1-110 kPa. Experiment set 1 had

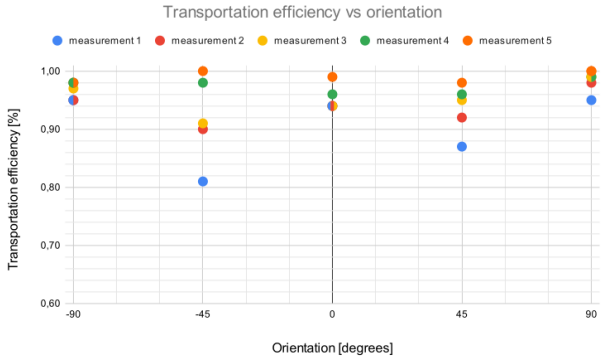

Fig. 29: Scatter plot displaying the influence of prototype orientation on the efficiency. Overlapping measurements are shown as multicoloured circles.

different conditions for tissue properties. An AVONA test on the results of this experiment set implied that tissue elasticity did not statistically affect transportation efficiency, confirming the compatibility of the prototype with diverse tissue types. A possible explanation for the transportation efficiency being independent on tissue shape is that half-cylindrical tissue phantoms have only half the amount of contact points with the wires compared to cylindrical phantoms, but also only half the weight, and thus half the transportation force is required. The effect of tissue stiffness on efficiency is presumed to be little as the tissue is not supposed to deform during transportation in a straight shaft.

The data showed variability in transportation efficiency during different experiment conditions. Taking all tissue transportation measurements including zero transport as 0% efficiency, an average efficiency of 75% was achieved, which does not satisfy the requirement of at least 90%. The low efficiency is mostly due to the prototype performing poorly during large curvature of the shaft. The prototype was able to perform the required curvature of 90 degrees over a shaft length of 80 mm, but was unable to transport tissue during large curvature of the shaft. During curvature, the cables straight-lined between two guiding points on the outside of the shaft, increasing contact force and friction. Due to this, the knots would get stuck on the guiding points of the rings, resulting in the prototype having low to zero transportation efficiency. This impacted the reliability as well, the average reliability over all experiments was 81%, a value below the desired goal of 90%.

Regarding the device orientation, this did not affect the transportation efficiency. The ANOVA test on the results of the experiments with varying prototype orientation yielded an insignificant result, implying that the transportation efficiency was independent of device orientation. Interesting to note is that the orientations of -45 and 45 degrees showed greater variability than the orientations of -90 and 90 degrees. A possible explanation for this is that the tissue phantoms during the (-)45 degree orientation would in some occasions come out of the shaft in a folded 'U' shape. This shape might have resulted from multiple factors during (-)45 degree orientation, that are different from horizontal or vertical orientation. A possible explanation would be lower friction at the front part of the tissue phantom due to gravitational force, while the back part would be pushed underneath the front to fold the phantom into the 'U' shape. The folded 'U' shape might result in higher friction between the shaft walls and tissue, and/or has a reduced number of contact points with the wires, which can result in lower transportation efficiency measurements.

The stiffness of the shaft could not be measured, as no machine was available to measure force and deflection. The dimensional requirements on the shaft were partially satisfied, the inner diameter was required to be equal or greater than 5 mm, the outer diameter equal or smaller than 10 mm and the shaft length equal or greater than 400 mm. The inner diameter was 6.1 mm, greater than 5 mm. The outer diameter of the shaft was 15 mm, this was due to limitations of FDM 3D-printing for the connection and add-on rings. The shaft length of the prototype was 215 mm, this was for ease of assembly. The shaft is constructed of two sections, two more sections can be added to increase the shaft length to satisfy the length requirement. However, the influence of a longer shaft on transportation efficiency was not investigated. It is hypothesised that a longer shaft leads to more friction on the wires, and thus a greater drive torque is necessary.

Regarding manufacturing of the prototype, the number of parts has been minimised using 3D-printing, creating complex parts that integrate multiple functions. All body parts fit onto each other by friction or shape, no single nut or bolt is used to connect the cone, tension ring, actuation base, drive ring, and cover to each other. An example of integrated functions is the drive ring, it drives the gears to power the prototype, while also protecting the gearbox from the outside environment. Regarding the operation of the prototype, the same prototype was used for all experiments, proving its reusability. However, damage to tissue occurred during transportation, as remains of tissue could be found on the wires and gears during experiments. If no method of cleaning is established, accumulation of tissue remains could impact the reusability and performance of the device. The tissue phantoms with 3 weight% were the most sensitive to damage, these phantoms experienced larger deformation due to their lower young's modulus compared to the 9 or 12 weight% phantoms.

The prototype is made of mostly PLA and stainless steel, both materials which are biocompatible. The tip is manufactured with Tough resin, but the part can be made biocompatible by manufacturing it using medical or dental resin with a biocompatibility certification. Besides the tip, the wire must be made of a different material to make the whole prototype suited for in-vivo surroundings. For the operation of the prototype, it is designed to be operated by a single user. The operator can use one hand to hold the prototype, and one hand to rotate the drive ring.

B. Limitations

The prototype was able to transport tissue using friction forces, but several design limitations were found after excessive operation. Wear and friction over time were not considered, especially inside the gearbox. The gears are manufactured using PLA, which is not a wear resistant material. The grip force between the teeth of the bevel gears can be reduced after high wear on the gears, leading to lower transmission of power. Furthermore, wear on the teeth of the spur gears contributes to a reduction in effective diameter over time, diminishing their ability to grip the wires and thus affecting transportation efficiency. Each of the six actuation units slides vertically through the actuation base with its guiding rods. Both the guiding rods and actuation base are made from PLA, wear can lead to more play between the rods and base. This can lead to misalignment, and actuation units touching each other, influencing the passive tension regulating mechanism. Besides wear, wire entanglement emerged as an issue. The wires sometimes tangled while sliding over the

knots connecting their ends. This problem is caused by the knots' thicker diameter compared to the wires. Besides, the knots impede smooth guidance of the wires through the shaft and gears. The knots would occasionally get stuck on an edge or hole for a short amount of time and increase friction. Sometimes, the knot would snap and make a wire useless.

The scope of this study did not include the procedure of tissue collection, insertion, and extraction from the prototype. Nevertheless, these procedures are important for functionality of the prototype. The prototype performed well executing tissue insertion. A small area of contact between the tissue phantom and wires resulted in enough friction to pull the tissue into the prototype. For tissue collection, a small tray was 3D-printed and used during experiments, but this does not offer a reliable long term solution. The extraction of tissue from the shaft proved challenging, the wires diverge at the end of the shaft and friction decreases between the wires and tissue. This led to the tissue being partially trapped within the shaft, as friction with the shaft was greater than friction with the wires. Softer tissues would sometimes stick to a single wire due to their softness and were then transported into the gears, which is undesired as the gearbox or tissue can suffer damage.

For ease of operation, the drive ring of the prototype was driven by hand. As the drive ring was operated by hand, it did not maintain a perfectly consistent rotation throughout all experiments. This resulted in varying transportation speeds and possibly a difference in slip. Slip can occur between the gears and wires, or between the wires and tissue. Similarly, tension on individual wires fluctuated during testing. Sometimes, wire knots would be stuck on an edge or in a hole for a short amount of time, this could have led to inconsistencies in tissue movement.

The results of the experiments are not only influenced by the dependent variables discussed in section V-C. During experiments, it became apparent that the stiffness of the gelatine tissue phantoms was dependent on gelatine weight%, but also highly dependent on ambient temperature. On a hot day, the tissue phantoms appeared much more soft than on a colder day. To limit this effect, all phantoms were kept in the fridge and only removed for immediate use. The time in the fridge also affected phantom stiffness, tissue phantoms became stiffer as time increased. Besides phantom stiffness, the phantom shape was not consistent. Phantoms were cut using a 3D-printed cutting tool, this resulted in non-perfect cylindrical and half-cylindrical shapes. Besides this, phantoms shrank significantly during longer periods of time in the fridge. Regarding the ANOVA tests, not many data points were used. Each group consists of five measurements, used to calculate the group means. As the ANOVA tests use little data points, no hard claims can be made about the results. The ANOVA test yielding an insignificant result only implies that the group means are equal, not that they in fact are.

C. Recommendations

The limitations of the prototype's current design impact its performance and long-term reliability. To enhance the performance and reliability of the prototype, several key improvements are recommended. Most of the prototype is now manufactured from PLA, as this was a cheap material with high availability. This material can be replaced by a more wear resistant material, which is still suitable for additive manufacturing such as ABS or PETG. For consistent rotation of the drive ring, a motor can be implemented into the device. This will also reduce the necessary actions for the operator of the device. To achieve long-term reliability and performance, a method of cleaning should be established as tissue remains were found in the prototype during experiments. Accumulation of tissue remains should be prevented, as it can reduce gear and wire performance over time.

For the wires, different solutions can be investigated to connect both ends, as the thick square knots limited device efficiency and reliability. Options are using a different type of knot, different material, different method of connection, or using a single wire over all gears. The fishing line used had very low friction on itself, a sturdy knot had to be used to prevent the knot from loosening itself. If a wire material with more friction on itself is used, a more simple knot can be used, which should be smaller than a square knot. Different materials also offer the possibility for a different method of connection, such as glueing or soldering instead of knotting. Another option is to use one long wire wrapped over all the gears, instead of twelve separate wires. One long wire only requires one square knot instead of twelve, but if it snaps, the device instantly loses functionality. When one or two of the twelve wires snapped, the device was still able to transport tissue through the shaft, but at the cost of lower transportation efficiency.

The shaft design can be improved for better guidance of the knots. During experiments with shaft curvature, the wires straight-lined between two guiding points on the outside of the shaft, leading to knots getting stuck and the device losing functionality. Figure 30 shows a suggestion for improvement, by increasing the amount of wire guiding points. By increasing the amount of guiding points, a bigger angle α occurs, which leads to a decrease in contact force between the wires and guiding rings. By adding rigid rings to the shaft, the flexibility decreases. A trade-off needs to be made, such that the shaft satisfies the bending requirement, while having a maximum number of guiding rings. Alternative manufacturing techniques should be explored for producing smaller shaft connection rings and add-on rings, as the rings of the prototype did not satisfy the required diameter using additive manufacturing. This was mainly due to resolution, minimum hole size and minimum wall thickness, indicated in Figure 31. Using precision manufacturing methods, such as CNC machining or laser cutting, could yield rings with finer tolerances and smoother surfaces, thereby reducing friction, reducing wall thickness, and improving the alignment of the shaft.

The actuation units can be redesigned to implement lubrication of the gears, lubrication would reduce driving friction and wear. The wires should not be contaminated with lubricant,

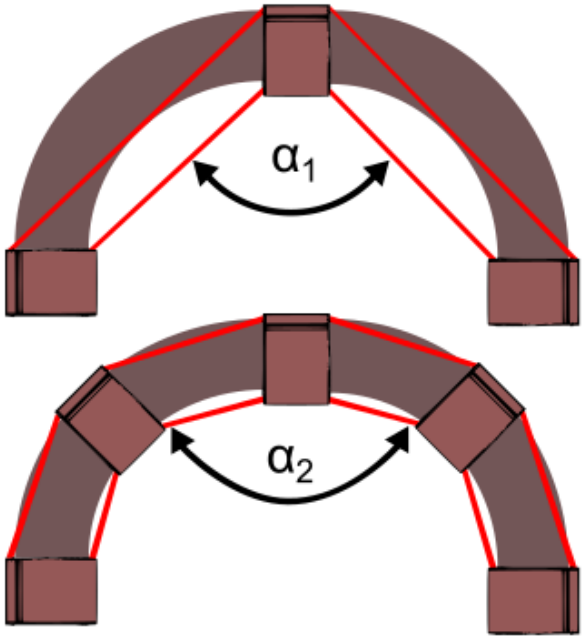

Fig. 30: Effect of multiple rings on angle α.

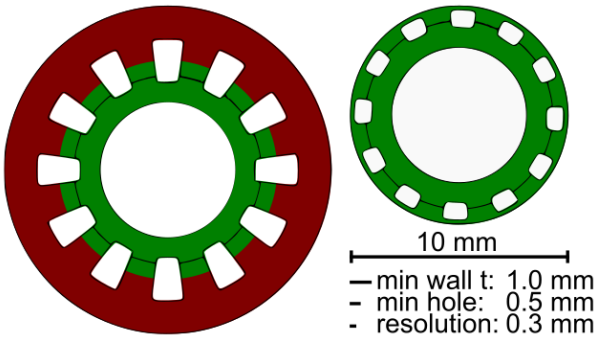

Fig. 31: Smaller rings are an option by using a different manufacturing technique rather than FDM 3D-printing.

this can be done by separation or increasing the distance between the gear bevel heads and the teeth that grip the wires. Figure 32 shows the current design and a possible adaptation suited for lubrication. The spur gears gripping the wires are moved behind the middle wall, such that they are shielded from the lubricated bevel heads. As the bevel head is split from the spur gear that grips the wire, the spur gear can be a different material. The bevel heads require a material that transmits the power well, while the spur gear can be of a rubbery material that provides more friction between the gear and the wires. An additional advantage of the extra wall is that the wire gripping wheels are in between two walls, such that the wires are constrained from both sides and cannot slide out the spur teeth into other gears. Moreover, this allows for possible sterilisation of the wires.

Overall, the developed device contributes to the advancement of the field of MIS by providing a novel friction-based

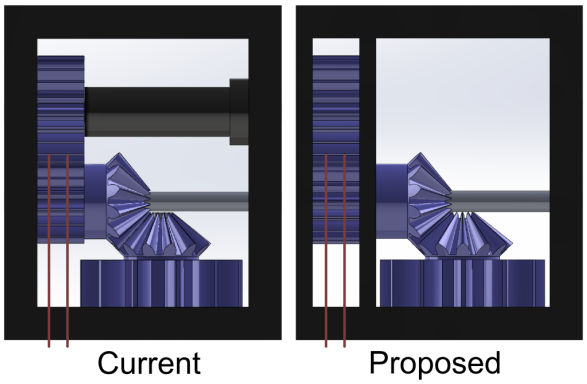

Fig. 32: Current design vs split gear design.

tissue transporting mechanism, addressing some of the limitations of current suction-based instruments. With the integration of the recommended improvements, both the performance and long-term reliability of the device can be enhanced. The enhanced device has the potential to improve procedures in MIS, ultimately contributing to improved patient outcomes.

VII. Conclusion

This study aimed to design and validate a flexible friction-based continuous tissue transporting device compatible with MIS. The transportation efficiency of the device should be independent of tissue elasticity within the Young's modulus range of 1-110 kPa. The manufactured prototype utilises friction to transport tissue inside its flexible shaft. Wires are wrapped around the shaft and translate continuously, creating a cylindrical conveyor belt. The prototype meets several key design requirements, including continuous transportation, transportation of tissue with different elasticity and shape, and a flexible shaft capable of navigating complex anatomical pathways. The prototype was evaluated on transportation efficiency during different conditions for tissue properties, shaft curvature, and device orientation. Experimental validation indicated that the transportation efficiency of the device is independent of tissue properties and orientation within the tested range, but the prototype's performance was significantly affected by shaft curvature. An average transportation efficiency of 75% was achieved during all experiment conditions. Furthermore, this study identified several limitations, such as tissue extraction, material wear, and wire entanglement, which impacted the reliability of the prototype. During all experiment conditions, 81% reliability was achieved, which is below the desired value of 90%. To enhance the prototype's performance and reliability, future work should focus on using wear-resistant materials for the gearbox, implementing a motor for consistent rotation, and exploring alternative methods for wire connection. Additionally, improving the shaft design to better guide the wires and knots during curvature will be crucial for the device performance. Overall, this study contributes to the advancement of the field of MIS by providing a novel friction-based tissue transporting mechanism that overcomes

some of the challenges of current suction-based instruments. Firstly, the device is less prone to clogging as friction forces cause transportation, rather than clogging the device. Secondly, friction forces to transport tissue are independent of shaft diameter, allowing easier miniaturisation compared to suction-based instruments. Thirdly, transportation efficiency is independent of tissue elasticity due to the use of a cylindrical conveyor belt mechanism. With further improvements, the developed device has the potential to improve the efficiency and reliability of tissue removal procedures in MIS, ultimately benefiting patient outcomes.

REFERENCES

[1] M. Spear, "The necessity of wound debridement," *Plast. Surg. Nurs.*, vol. 30, no. 1, pp. 54–56, 2010.

[2] M. H. Meissner, "Rationale and indications for aggressive early thrombus removal," *Phlebology*, vol. 27, pp. 78–84, 2012.

[3] T. Jaschinski, C. Mosch, M. Eikermann, and E. A. Neugebauer, "Laparoscopic versus open appendectomy in patients with suspected appendicitis: a systematic review of meta-analyses of randomised controlled trials," *BMC Gastroenterol*, vol. 15, no. 1, 2015.

[4] T. N. Robinson and G. V. Stiegmann, "Minimally invasive surgery," *Endoscopy*, vol. 36, pp. 48–51, Jan. 2004.

[5] A. Sakes and et al., "Development of a novel wasp-inspired friction-based tissue transportation device," *Frontiers in Bioengineering and Biotechnology*, vol. 8, 2020.

[6] E. P. de Kater et al., "Design of a flexible wasp-inspired tissue transport mechanism," *Frontiers in Bioengineering and Biotechnology*, vol. 9, 2021.

[7] G. Rioufol, B. Collin, M. Vincent-Martin, P. Buffet, L. Lorgis, I. L'Huillier, and et al., "Large tube section is the key to successful coronary thrombus aspiration: findings of a standardized bench test," *Cathet. Cardiovasc. Intervent.*, vol. 67, no. 2, pp. 254–257, 2006.

[8] J. Madjidyar and et al., "Influence of thrombus composition of thrombectomy: adapt vs. balloon guide catheter and stent retriever in a flow model," *Röfo - fortschritte auf dem gebiet der röntgenstrahlen und der bildgebenden verfahren*, vol. 192, pp. 257–263, Mar. 2020.

[9] Y. Shi and et al., "Suction force-suction distance relation during aspiration thrombectomy for ischemic stroke: a computational fluid dynamics study," *Physics in Medicine*, vol. 3, pp. 1–8, Jun. 2017.

[10] Y. C. Hu and M. F. Stiefel, "Force and aspiration analysis of the adapt technique in acute ischemic stroke treatment," *J. Neurointervent. Surg.*, vol. 8, no. 3, pp. 244–246, 2016.

[11] Y. Verberne and et al., "The design of a friciton-based tissue transportation mechanism for minimally invasive surgery," *Delft University of Technology Repository*, Sep. 2022.

[12] K. Comley and N. A. Fleck, "A micromechanical model for the young's modulus of adipose tissue," *International Journal of Solids and Structures*, vol. 47, pp. 2982–2990, Oct. 2010.

[13] K. Arda and et al., "Quantitative assessment of normal soft-tissue elasticity using shear-wave ultrasound elastography," *American Journal of Roentgenology*, vol. 197, pp. 532–536, Sep. 2011.

[14] M. Li and et al., "Vine catheter for endovascular surgery," *IEEE Transactions on Medical Robotics and Bionics*, vol. 3, pp. 384–391, May 2021.

[15] C. Brandt-Wunderlich and et al., "Cardiovascular catheter stiffness - a static measurement approach," *Current Directions in Biomedical Engineering*, vol. 7, no. 2, pp. 721–723, 2021.

[16] X. Yu and et al., "Needle-shaped ultrathin piezoelectric microsystem for guided tissue targeting via mechanical sensing," *Nature Biomedical Engineering*, vol. 2, pp. 165–172, Mar. 2018.

[17] T. D. Long and et al., "Novel aspiration catheter design for acute stroke thrombectomy," *Journal of NeuroInterventional Surgery*, vol. 11, pp. 190–195, Feb. 2019.

[18] S. R. C. Driessen and et al., "Electromechanical morcellators in minimally invasive gynecologic surgery: An update," *Journal of Minimally Invasive Gynecology*, vol. 21, pp. 377–383, May 2014.

[19] Y. Han, Y. Uno, and A. Munakata, "Does flexible small-diameter colonoscope reduce insertion pain during colonoscopy?," *World Journal of Gastroenterology*, vol. 6, pp. 659–663, Oct. 2000.

[20] Olympus Europa, "Moresolution laparoscopic power morcellator: tissue extraction," *https://www.olympus-europa.com/medical/en/Products-and-Solutions/Products/Product/moresolution.html*, May 2022, visited 30-10-2023.

[21] A. Karimi and M. Navidbakhsh, "Material properties in unconfined compression of gelatin hydrogel for skin tissue engineering applications," *Biomedizinische Technik. Biomedical Engineering*, vol. 59.6, pp. 479–486, Dec. 2014.

Appendix A
Design Wishes

Transportation wishes

1) *Transportation efficiency:* The transportation efficiency does not vary statistically between different tissues in the elasticity range of 1-110 kPa
2) *Transportation efficiency:* The transportation efficiency is maximised with a minimum of 90%
3) *Reliability:* The reliability of the device is 100%
4) *Shaft orientation:* The operability of the device is independent of the shaft orientation
5) *Manufacturability:* The number of components is minimised

Procedure wishes

6) *Working length:* The device is suitable for a working length of 1.25 m [17]
7) *Durability:* The device is reusable
8) *Internal damage risk:* The device does not damage transported tissue
9) *Biocompatibility:* The device is biocompatible for in-vivo surroundings
10) *Handling:* The device can be operated by a single user

Appendix B
In-depth Analysis of Device by Verberne et al.

Figure 33 shows an exploded view of the device developed by Verberne et al. [11], the different components fulfil different functions, the most important functions will be discussed. The inner tube enables tissue transportation by forming the transportation lumen (F1). The gear base and gears have the function to enable continuous thread rotation (F3). The wire loops are tensioned and clamped over the revolving small gears (C8). The internal gear can be rotated by human hand or by an electric motor, it actuates the whole system. The small gears shift the axis of revolution by 90 degrees. This shift is necessary as the wires loop around the inner tube in a plane perpendicular to the plane of actuation. The tip, spacer, and cone enable smooth actuation, these components guide the wires along the desired paths and minimise undesirable friction (F4). The tip leads to a larger radius to prevent kinks when the wires are guided along the tip. The spacer creates an offset between the wires and the outside of the inner tube, decreasing contact area and friction. Besides, it distributes the wires equally to prevent wires touching each other. The cone connects the small diameter of the shaft to the gear base with a larger diameter; it guides the separation of the wires.

The gears, cone, and tip ensure that all wire positions remain the same during operation and do not get tangled (F5). Tension is very important for the actuation of the wires, as tension creates friction with the small gears. The cap is used to tension all wires simultaneously by in- or decreasing the distance between the cone and the gear base (F6). Manufacturability and assembly by hand were important requirements for this

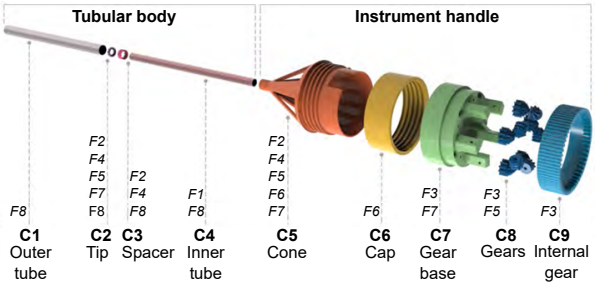

Fig. 33: Exploded view of the components of the friction-based tissue transporting device and corresponding functionalities (F) developed by Verberne et al. [11]. Enable tissue transport (F1). Enable thread connection (F2). Enable continuous thread rotation (F3). Enable smooth actuation (F4). Ensure thread position (F5). Ensure thread tension (F6). Ensure manufacturability (F7). Ensure MIS compatibility (F8).

device (F7). The tip, cone, and gear base need to be fixed with respect to each other, afterwards the thread can be inserted, tied, and tensioned. The gearbox is positioned on the outside of the gear base, as this is for easy access during assembly. To make the device compatible with MIS (F8), the outer tube should have a maximum diameter of 10 mm and the inner tube a minimum diameter of 5 mm. All materials that enter the human body need to be resistant to the human body fluids they might encounter. Besides, the materials used should not pose any danger to the patient's health. Both tubes are made from stainless steel, the outer tube prevents surrounding tissue from contact with the moving parts of the device to increase safety.

Appendix C
Final Prototype Parts

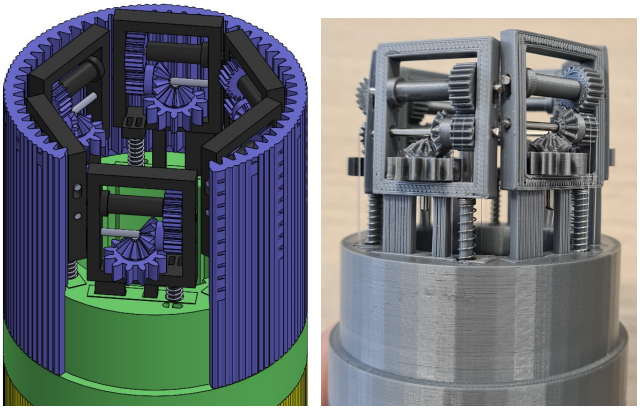

Fig. 34: Designed and manufactured actuation units.

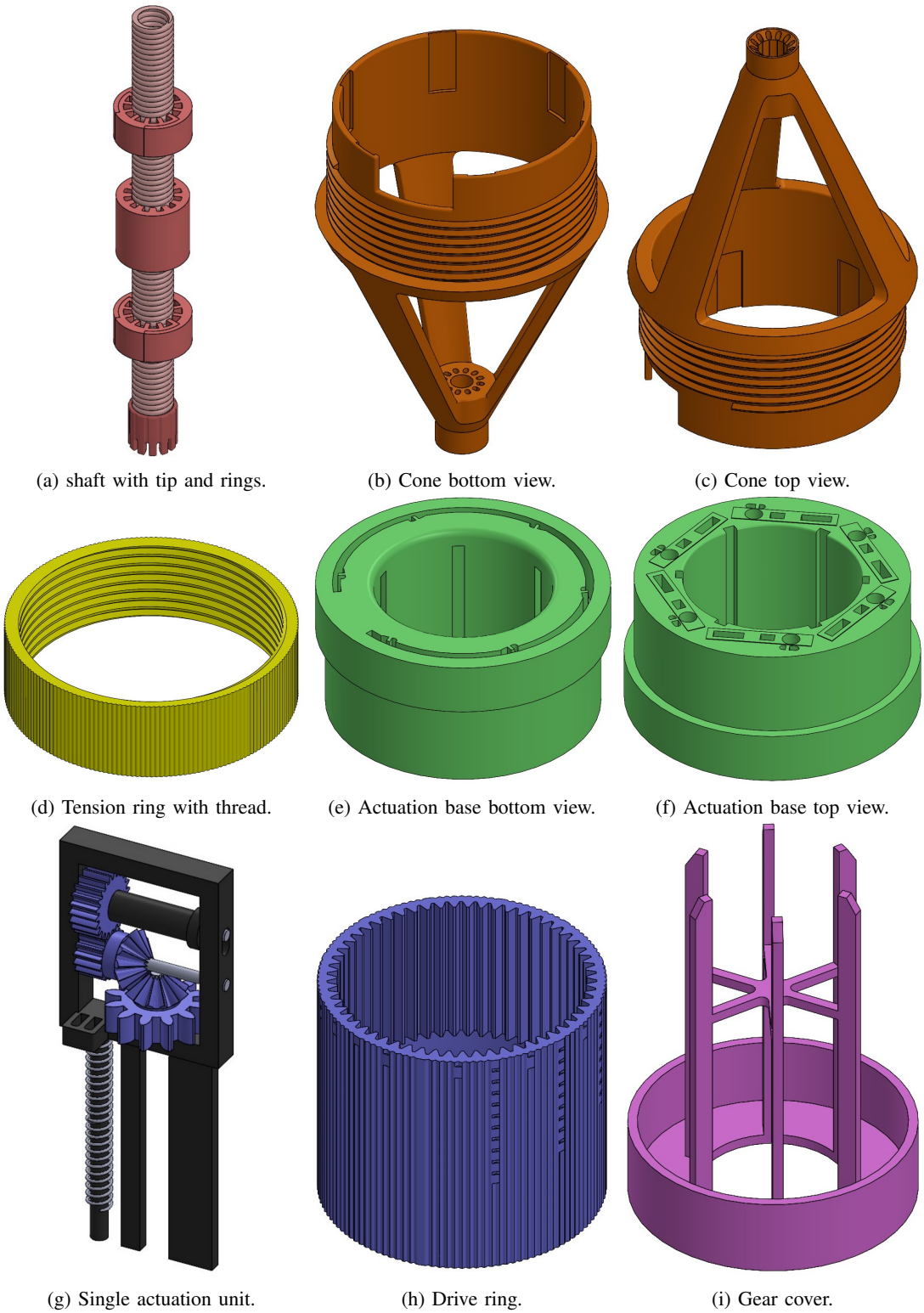

(a) shaft with tip and rings. (b) Cone bottom view. (c) Cone top view.

(d) Tension ring with thread. (e) Actuation base bottom view. (f) Actuation base top view.

(g) Single actuation unit. (h) Drive ring. (i) Gear cover.

Fig. 35: All prototype parts in different views.

Appendix D
Design Iterations

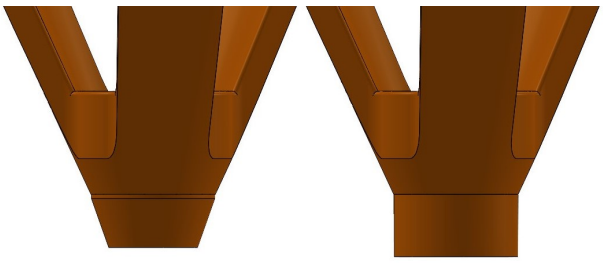

Fig. 36: Cone tip design versus manufactured cone.

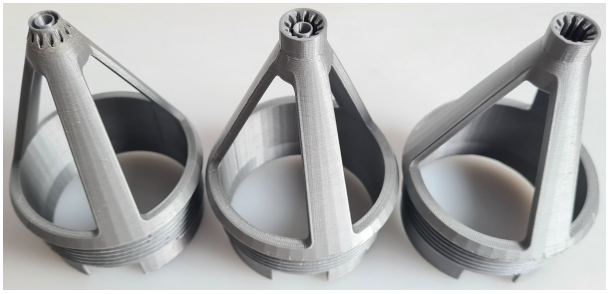

Fig. 37: Different iterations of the cone.

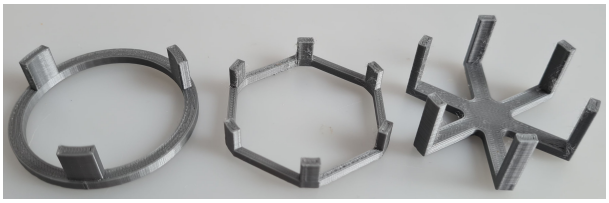

Fig. 38: Different iterations of clamping pins for the cover.

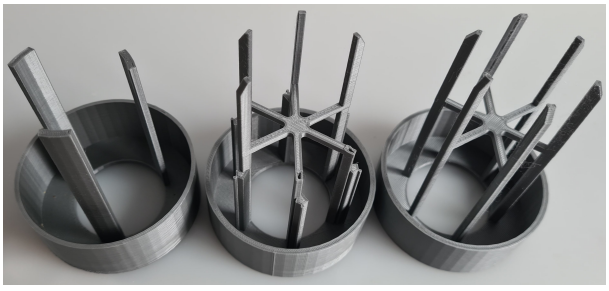

Fig. 39: Different iterations for the cover.

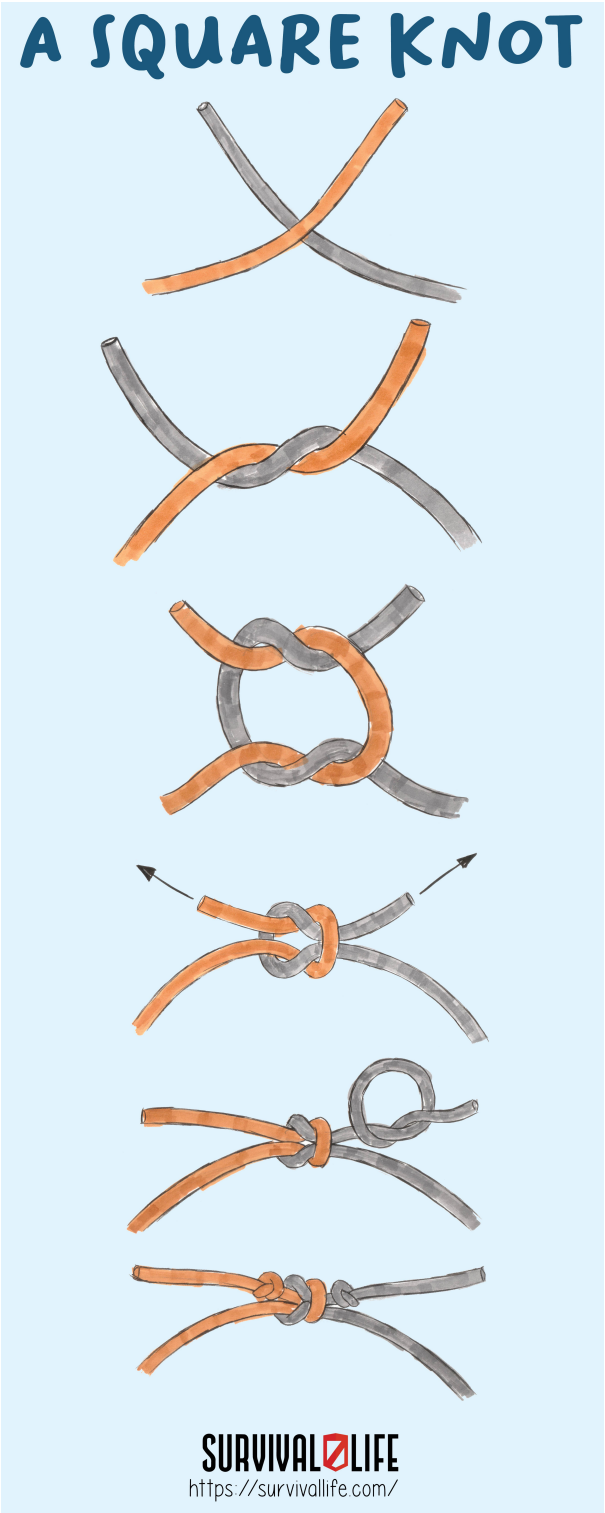

Fig. 40: Square knot used for connecting the wire ends.

APPENDIX E
EXPERIMENTS

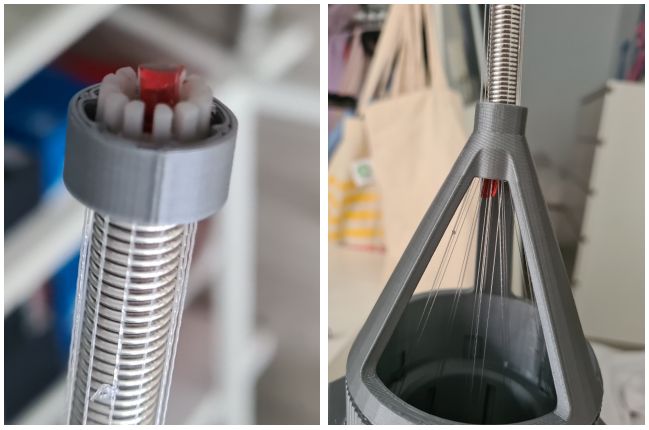

(a) Phantom entering the shaft. (b) Phantom exiting the shaft.

Fig. 41: Tissue phantom entering and exiting the shaft during experiments.

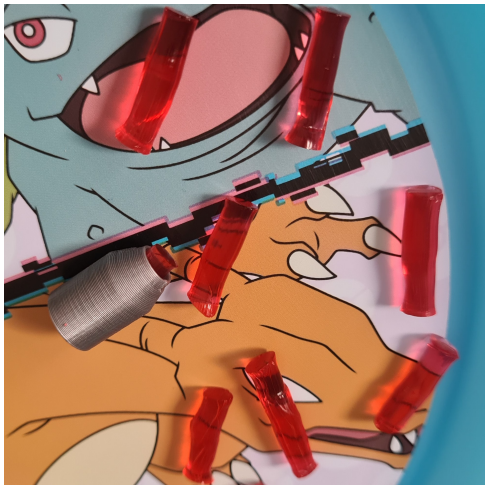

(a) Gelatin phantoms and cutting tool.

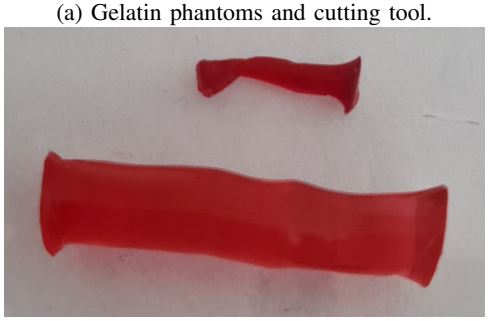

(b) Gelatin shrinks after a few nights in the fridge.

Fig. 42: Gelatin phantoms and importance of shrinkage.